8

Thermohaline staircases

Oceanographers tend to get a bit emotional when discussing thermohaline staircases. The literature on this subject is sprinkled with colorful epithets – staircases are "dramatic," "spectacular," "striking" and "easy to admire." The reason why otherwise restrained and business-like folks suddenly become so passionate and poetic is clear from just a brief look at the structure of staircases. Thermohaline staircases (Fig. 8.1) consist of remarkably regular homogeneous layers in vertical temperature and salinity profiles. Although these mixed layers are tens of meters deep, they are created and maintained by double-diffusive processes operating on a centimeter scale. It is the ocean falling on its knees at the first sight of an army of merciless salt fingers; it is a complete surrender of large scales to the tiniest ones. Why would Nature, usually predisposed to turbulent and disorganized geophysical flows, create something so strangely precise and elegant?

It is no surprise that such an intriguing phenomenon has attracted continuous attention from observationalists and theoreticians alike. The first observations of staircases in the ocean were reported in the late 1960s (Tait and Howe, 1968; Cooper and Stommel, 1968) and were followed by a stream of similar measurements from various locations. The link between staircases and double-diffusion was recognized almost immediately and was widely and painlessly accepted by the oceanographic community. During the same period, staircases were reproduced in the laboratory (Turner, 1967; Stern and Turner, 1969), which stimulated new ideas on their dynamics. Almost there, right? It only remained to identify the exact mechanics of staircase generation, beyond the vague "salt fingers did it" level. Double-diffusers never made this final step. More than forty years later, we are still debating the relevance of at least half a dozen different layering mechanisms. Staircase dynamics is a subject filled with mysteries and speculations.

Our discussion of staircases starts with some key oceanographic observations (Section 8.1) and is followed by a summary of different hypotheses for their origin (Section 8.2). Our intentions are two-fold. First, we wish to offer readers an unbiased view on the subject. It is also important to realize that the evolution

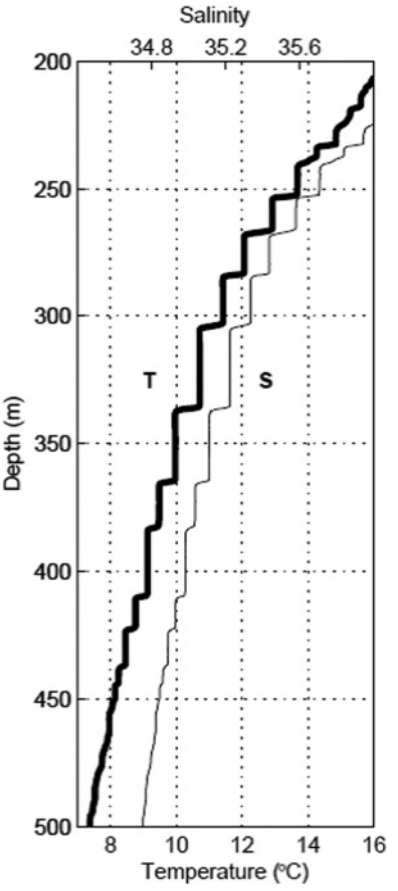

Figure 8.1 Typical profiles of potential temperature and salinity in the tropical Atlantic staircase taken during the SFTRE program. From Schmitt *et al*. (2005).

of complex systems in the ocean is usually governed by a combination of several processes. Very rarely is there only one explanation for anything that is remotely complicated in fluid dynamics and there may well be elements of truth in each staircase theory. The most recent model, and the author's favorite – the instability of the flux-gradient laws – is discussed in greater detail afterward (Section 8.3). We end the chapter by discussing the salient evolutionary features of fully developed staircases in Section 8.4.

8.1 Observations

Salt-finger staircases

The majority of observations of salt-finger staircases have come from three locations: the western tropical Atlantic (Schmitt *et al*., 1987, 2005), Tyrrhenian Sea

(Zodiatis and Gasparini, 1996), and the Mediterranean outflow in the northeast Atlantic (Tait and Howe, 1968, 1971; Magnell, 1976). The common feature of these regions is the anomalously low values of density ratio, which appears to be both necessary and sufficient for staircase formation. No staircases have been reported for $R_\rho > 2$ and the reduction of density ratio below 1.7 is inevitably associated with the appearance of step-like structures in vertical T–S profiles (Fig. 8.2). The spatial pattern of staircases is also very sensitive to R_ρ. As the density ratio decreases, staircases become more pronounced and the height of steps sharply increases. This connection is significant. The density ratio is the single most important parameter controlling the intensity of salt fingers and the sensitivity of staircases to variations in R_ρ is one of many signs that staircases are a product of double-diffusion.

More direct evidence for the double-diffusive origin of staircases includes optical observations of salt fingers in interfacial regions using shadowgraph systems, as in Figure 8.3. Images of salt fingers from the Mediterranean outflow staircases bear striking resemblance to the laboratory shadowgraphs (bottom panel of Fig. 8.3). Shadowgraphs taken in the western tropical Atlantic during the C-SALT (Caribbean Sheets and Layers Transect) program also show well-defined salt fingers, frequently tilted by large-scale shear. Microstructure measurements in the interfaces (Magnell, 1976; Gregg and Sanford, 1987; Schmitt *et al.*, 2005) reveal all the expected signatures of salt-finger dynamics. The spectrum of the thermal signal is usually narrow-band, and the spectral peak corresponds to the wavelengths of the fastest growing finger modes. The scaled ratio of thermal variance and energy dissipation is high (recall that fingers are effective mixers of temperature but poor mixers of momentum), which rules out mechanical turbulence as a dominant source of dissipation.

The most recent and, in my opinion, incontrovertible proof of double-diffusive dynamics of staircases comes from the Salt Finger Tracer Release Experiment (SFTRE). During the cruise of 2001, 175 kg of sulfur hexafluoride (SF_6) was released in the interior of the Caribbean staircase. The molecular diffusivity of SF_6 and salt are close and therefore the mixing rate of salinity, which is otherwise difficult to measure, was inferred from the vertical spreading of the tracer. The observed dispersion rates imply an effective vertical diffusivity of salt of $K_S = (0.85 \pm 0.05) \cdot 10^{-4}\,\mathrm{m^2\,s^{-1}}$, which significantly exceeds the temperature diffusivity measured at the same location, $K_T = (0.45 \pm 0.2) \cdot 10^{-4}\,\mathrm{m^2\,s^{-1}}$ – a clear signature of salt fingering. The corresponding flux ratio for the typical density ratio of $R_\rho \approx 1.6$ is

$$\gamma = \frac{F_T}{F_S} = \frac{K_T}{K_S} R_\rho \approx 0.85. \tag{8.1}$$

The flux ratio expected for salt fingers on the basis of DNS, experiments and linear theory (see Fig. 2.7a) is $\gamma_{\mathrm{sf}} \approx 0.6$ – somewhat less than (8.1) but definitely within

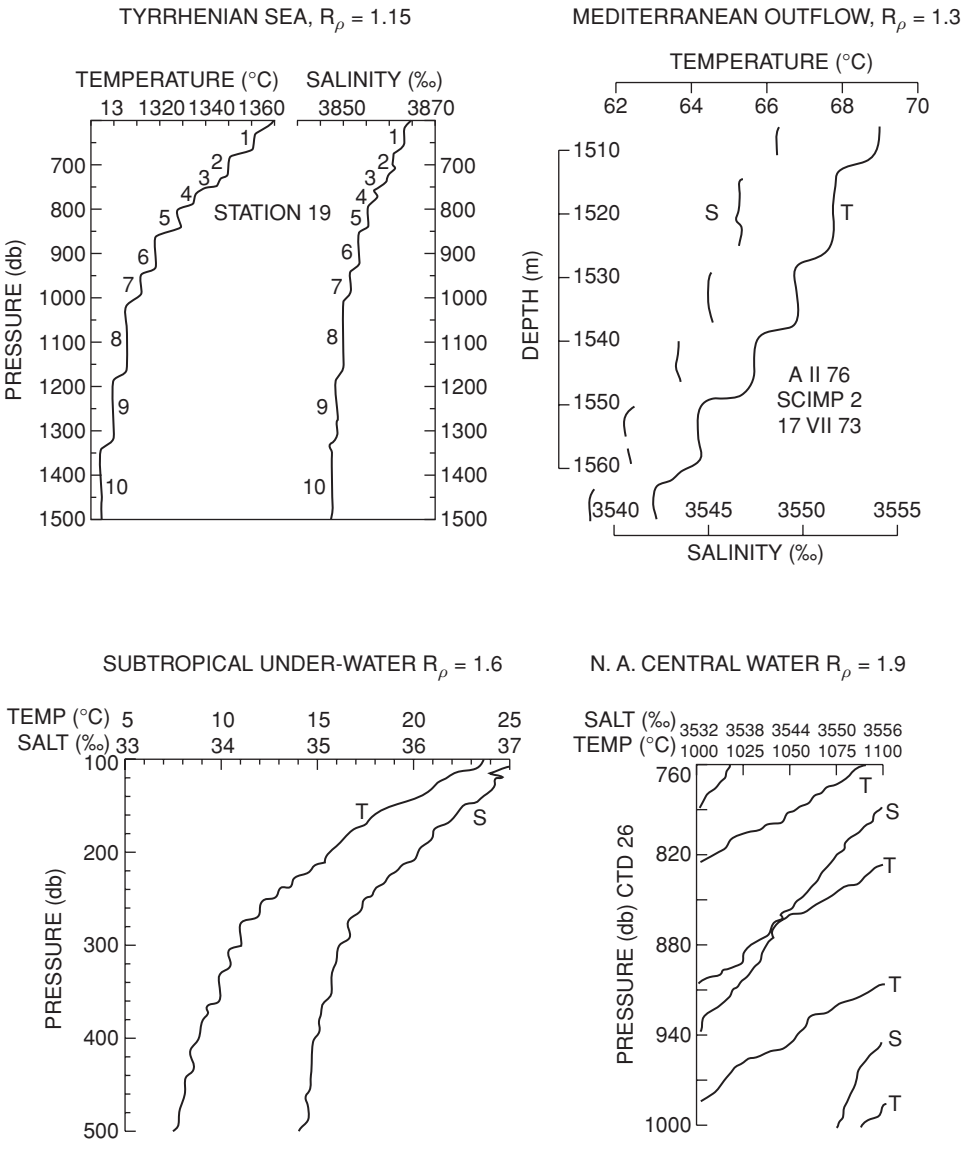

Figure 8.2 Examples of thermohaline staircases from various locations. Note the tendency of staircases to become more pronounced as the density ratio decreases. Redrawn from Schmitt (1981).

a margin of error. The discrepancy could be readily attributed, for instance, to the nonlinearities in the equation of state (McDougall, 1991). The flux ratio in (8.1) cannot be produced by any known mixing process in the ocean except for double-diffusion. For turbulence, which tends to mix heat and salt at equal rates, the

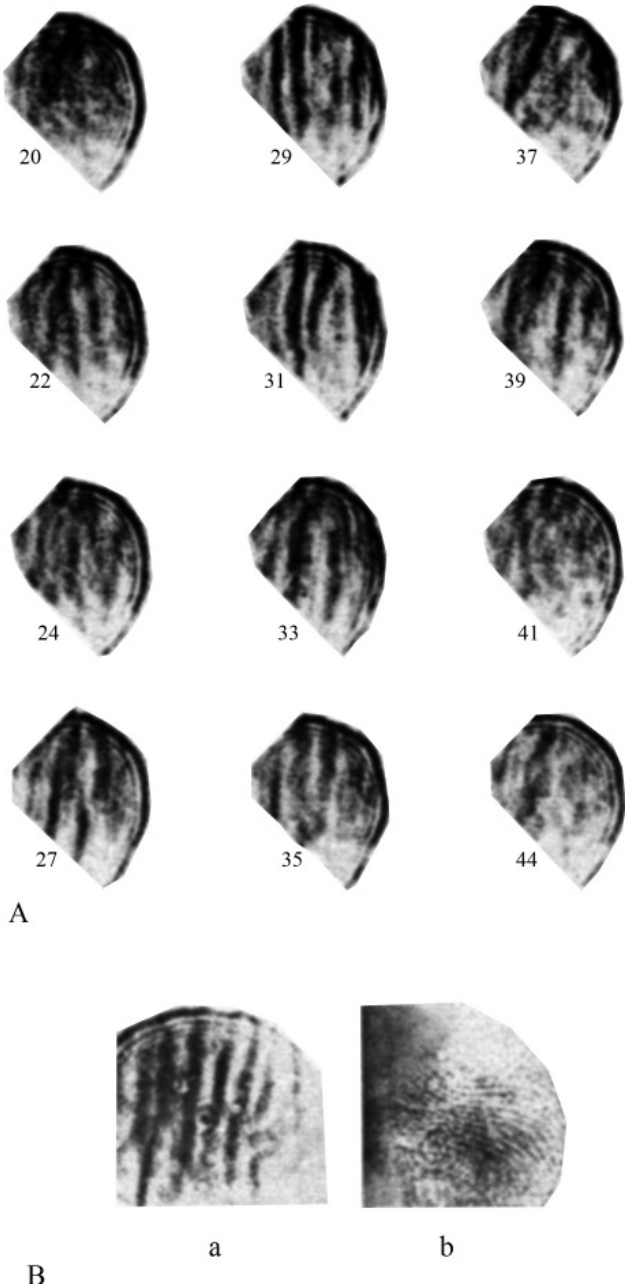

Figure 8.3 (A) Shadowgraph images of salt fingers in the Mediterranean outflow. The dark bands are shadows of descending fingers (high refractive index) and the light bands are shadows of rising fingers (low refractive index). (B) Shadowgraph images in a laboratory tank. Image (a) shows salt fingers. Image (b) is a blank pattern after the tank was stirred. From Williams (1974).

corresponding flux ratio would be much higher ($\gamma_{\text{turb}} = R_\rho \approx 1.6$). The secondary role of turbulence can be further ascertained by parameterizations based on the intensity of the gravity wave field at this location. The level of turbulent mixing supported by waves ($K_{\text{turb}} \approx 0.02 \cdot 10^{-4}\,\text{m}^2\,\text{s}^{-1}$) does not even come close to the actual diffusivities of salt or heat.

The three-dimensional structure of staircases is also of interest. Several layers in the Caribbean staircase were found to be coherent over lateral distances exceeding 100 km. Figure 8.4a shows a series of consecutive profiles separated by 1.3 km within the total distance of 33 km. The spatial continuity of the Caribbean staircase is impressive, particularly given the high levels of mesoscale variability at this location and associated strong time-dependent shears, both horizontal and vertical. The interfaces tilt at a finite angle relative to the isopycnal surfaces, which is revealed most clearly by the T–S diagram in Figure 8.4b. The temperature and salinity values for each mixed layer are aligned along the curves corresponding to a remarkably uniform lateral density ratio of $R_l = \frac{\alpha \Delta T_{\text{layer}}}{\beta \Delta S_{\text{layer}}} = 0.85 \pm 0.02$ in spring and $R_l = 0.84 \pm 0.03$ in autumn. Here, $\left(\Delta T_{\text{layer}}, \Delta S_{\text{layer}}\right)$ represent the lateral variation in temperature and salinity within each mixed layer.

The observed value of the lateral density ratio in the mixed layers can be rationalized from the balance between the lateral advection in mixed layers and convergence of the vertical small-scale eddy fluxes of heat and salt:

$$\begin{cases} \vec{\mathrm{v}} \cdot \nabla T = -\dfrac{\partial F_T}{\partial z}, \\ \vec{\mathrm{v}} \cdot \nabla S = -\dfrac{\partial F_S}{\partial z}. \end{cases} \tag{8.2}$$

If the flux ratio is relatively uniform $\alpha F_T = \gamma \beta F_S,\ \gamma \approx const$, then

$$\vec{\mathrm{v}} \cdot (\alpha \nabla T - \gamma \beta \nabla S) = 0, \tag{8.3}$$

which, in turn, implies that the downstream variations in temperature and salinity are linked:

$$R_l = \frac{\alpha \Delta T_{\text{layer}}}{\beta \Delta S_{\text{layer}}} \approx \gamma. \tag{8.4}$$

Equation (8.4) affords an alternative estimate of the flux ratio: $\gamma \approx R_l \approx 0.85$ in agreement with (8.1). Such consistency of two independent observation-based estimates lends credence to our interpretation of the results in Figure 8.4b. The cross-flow variation in properties is more difficult to predict. However, it is not unreasonable to speculate that lateral mixing in layers tends to homogenize water masses in the direction normal to the advecting velocity and therefore all measurements of temperature and salinity in individual layers collapse on the distinct

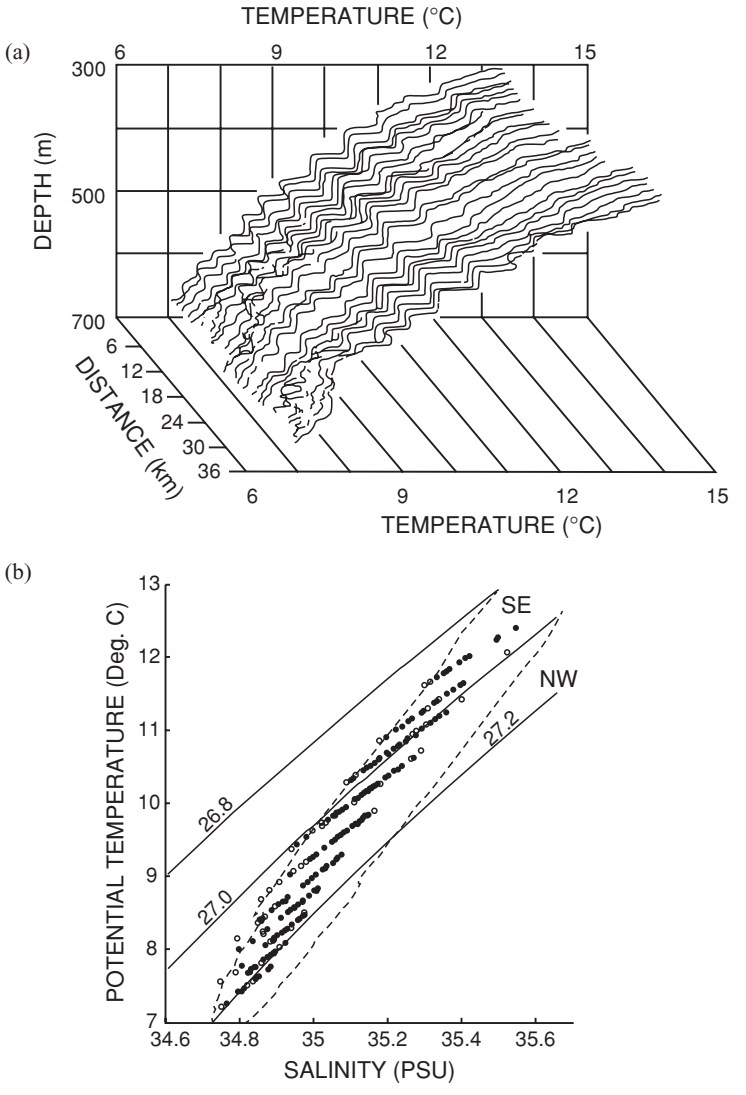

Figure 8.4 (a) Three-dimensional view of the offset temperature profiles taken during the C-SALT experiment. (b) Potential temperature–salinity values of the C-SALT layers. The solid circles are from mixed layers more than 10 m thick, the open circles are from layers 5–10 m thick. Also shown are the *T*–*S* relations at the northwest and southeast corners of the survey area (dashed curves) and isopycnal surfaces (solid curves). From Schmitt *et al*. (1987).

curves clearly visible in the *T*–*S* diagram (Fig. 8.4b). What is most striking in this story is the extent to which the data in Figure 8.4b conform to (8.4). The lateral density ratio in layers is uniform to within a fraction of a percent – something as firm and consistent is rarely found in oceanographic field measurements.

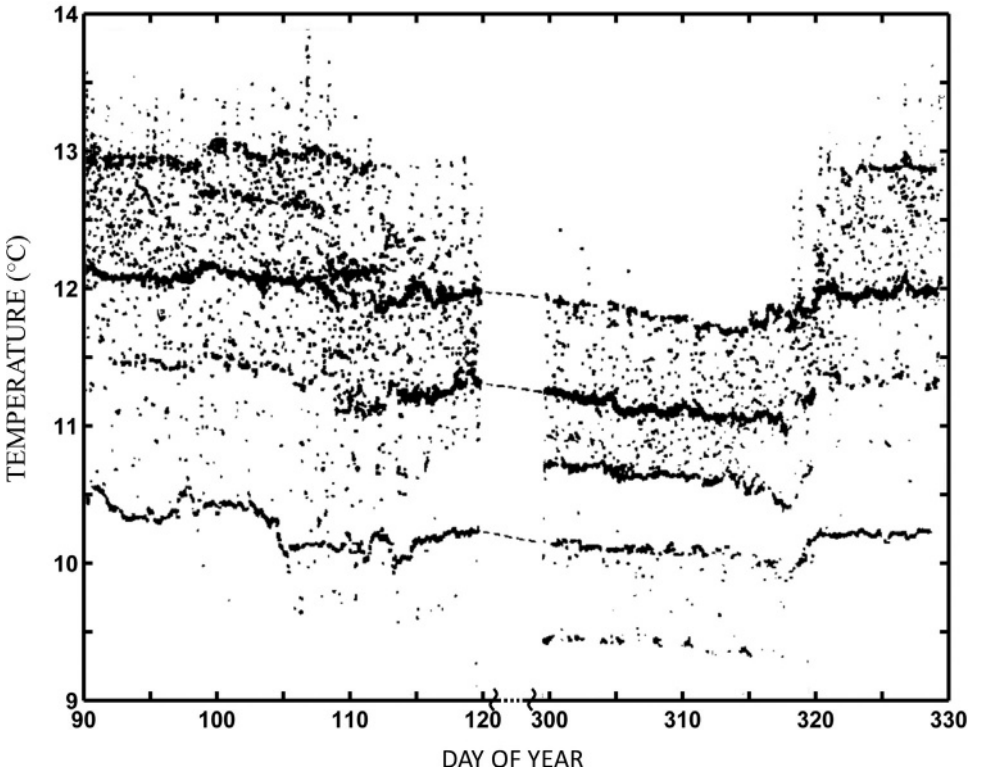

Figure 8.5 Temperature recorded at the mooring site in the C-SALT area in the depth range 325–415 m. Only the first and last 30 days are shown from a continuous eight-month record, as the character of the data does not change during the intervening time. Well-mixed layers appear as heavy concentrations of points, three of which may be traced through the entire record. From Schmitt *et al*. (1987).

The analysis of temporal variability in fully developed staircases reveals their persistence and structural stability. Figure 8.5 presents a continuous record of the vertical temperature profile at the mooring deployed for eight months during C-SALT (Schmitt *et al*., 1987). Several well-defined layers maintained their identity throughout the entire period of observation, despite the significant short-term variability associated with gravity waves and mesoscale eddies. Figure 8.6 offers a glimpse into the evolutionary dynamics on even longer time scales. It shows a series of temperature and salinity profiles taken in the Tyrrhenian staircase during the period from 1973 to 1992. Two features should be emphasized. Several interfaces in Figure 8.6 can be identified, by their location and *T*–*S* values, in profiles taken several years apart – a testament to the remarkable resilience of thermohaline staircases. However, occasionally interfaces disappear, resulting in the systematic merging of the adjacent mixed layers. Figure 8.6 shows ten layers in the 1973

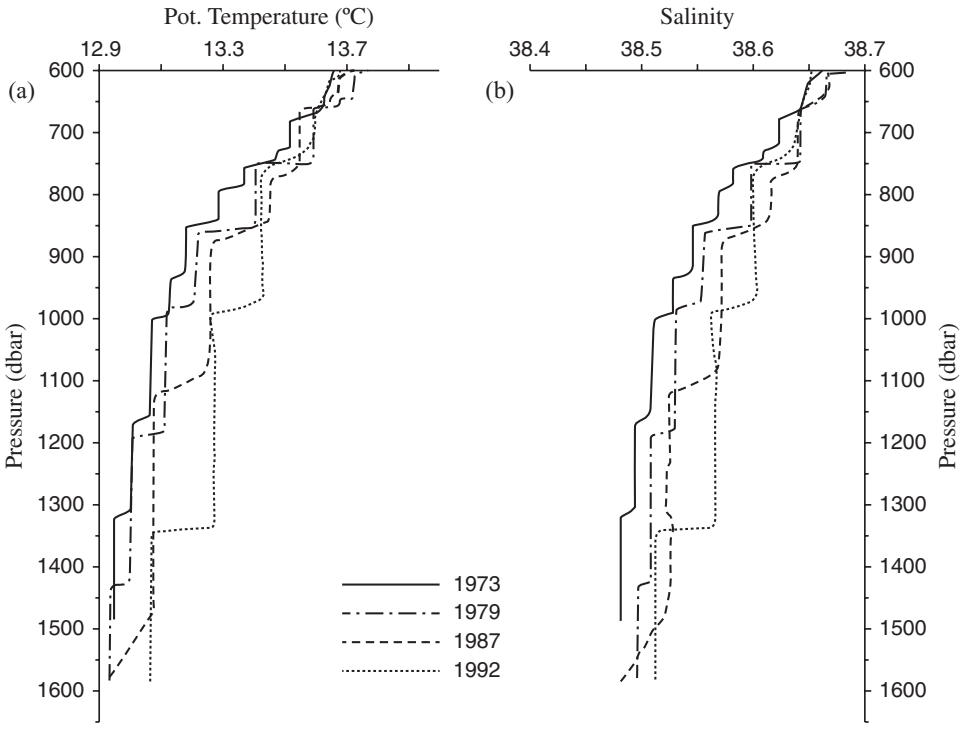

Figure 8.6 (a) Potential temperature and (b) salinity profiles in the central Tyrrhenian basin over a 19-year period. From Zodiatis and Gasparini (1996).

profiles but only four spectacular layers several hundred meters thick are present in 1992. The dynamical mechanisms and ramifications of layer-merging events will be discussed in Section 8.4.

Generally, staircases are not expected to occur in the coastal environment. Strong shears and elevated levels of turbulence near topographic boundaries are usually quite effective in preventing spontaneous layering. However, a curious counterexample has been reported recently. Spear and Thomson (2012) present evidence of a well-defined staircase in Belize Inlet, a British Columbia fjord. Hydrographic measurements suggest an intrusion of cold and fresh oceanic water into the fjord, which created finger-favorable conditions above its level (∼150 m) and diffusive conditions below. Salt-finger staircases were observed in the depth range of 70–150 m with step heights of approximately 10 m. Diffusive layers formed in the depth range 150–210 m and were much smaller (∼1 m). This example illustrates the ability of thermohaline staircases to withstand substantial levels of adverse ambient forcing, associated in Belize Inlet with strong tidally induced shears and turbulence.

An interesting perspective on the dynamics of staircases is afforded by seismic imaging, a new ocean-observing technology briefly described in Chapter 7. Staircases are particularly suitable for seismic analysis because of (i) the strong reflectivity of high-gradient interfaces, (ii) layer scales that are easily resolved by seismic inversion and (iii) limited horizontal variability. Biescas *et al*. (2010) presents a series of spectacular images of the salt-finger staircase formed below the Mediterranean outflow. In Figure 8.7a, the staircase is visibly perturbed by internal waves and yet remains well-defined and spatially coherent. The interaction with a meddy (Fig. 8.7b) offers another example of the resilience of the staircase. Layers are disorganized in the immediate vicinity of the meddy but remain remarkably regular on the outside. In Figure 8.7c, the staircase is disrupted by the elevated turbulent mixing near a topographic boundary, but the damage is contained within the local area of interaction. A similar seismic image of a region occupied by the Caribbean (C-SALT) staircase (Fer *et al*., 2010) is shown in Figure 8.8. Once again, acoustic detection tells the story of a staircase struggling to maintain its structure and coherence in the face of external disturbances.

Diffusive staircases

Whilst salt-finger staircases have been the subject of continuous scrutiny since their discovery, diffusive staircases, on the other hand, have historically received less attention. One of the reasons is related to their prevalence in high-latitude locations, where field programs are more demanding. The first documented observations of diffusive staircases were made by Neal *et al*. (1969), whose vertical temperature profiles from the central Arctic revealed regular step-like patterns (Fig. 8.9) in the region overlying relatively warm and salty waters of Atlantic origin. The layering was promptly attributed to double-diffusion and dynamic parallels with salt-finger staircases (Tait and Howe, 1968) were drawn. Aside from the opposite sign of the background temperature and salinity gradients, diffusive staircases in the Arctic are characterized by much smaller steps. Both the thickness and particularly the variation in properties across the steps are much less than in typical salt-finger staircases (see Table 8.1). Subsequent field programs (Neshyba *et al*., 1971; Neal and Neshyba, 1973; Perkin and Lewis, 1984) revealed that staircases are ubiquitous in the Arctic and are likely to affect the high-latitude water-mass distribution (e.g., McDougall, 1983).

Arctic staircases were explored more systematically during the Arctic Internal Wave Experiment (AIWEX). Padman and Dillon (1987, 1988, 1989) found that staircases in the central Arctic (Canada Basin) were located between 320 and 430 m depth, with steps 1–2 m thick and temperature jumps across interface in the range $0.004\ ^\circ\mathrm{C} < \Delta T < 0.012\ ^\circ\mathrm{C}$. The corresponding vertical heat fluxes

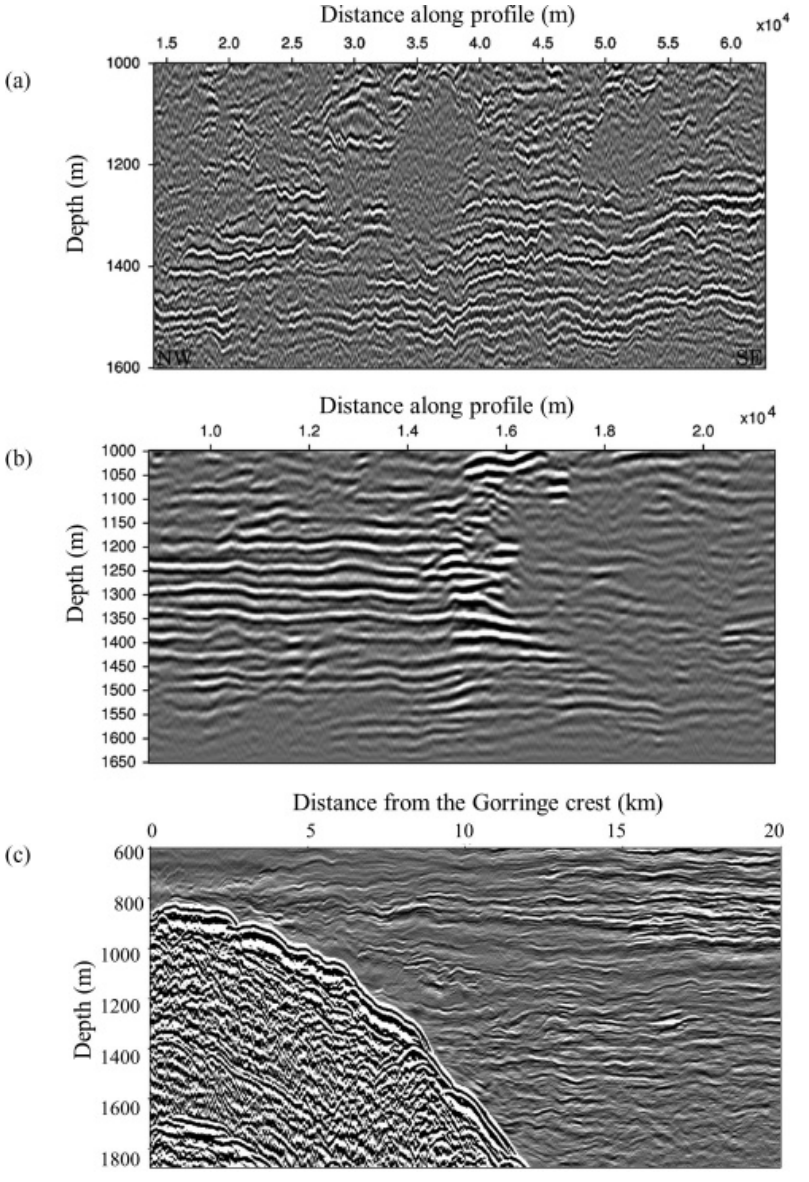

Figure 8.7 Seismic images of the Mediterranean outflow staircase. The staircase in (a) is perturbed by internal waves, in (b) interacts with a meddy and in (c) interacts with the topographic boundary. From Biescas *et al.* (2010).

evaluated using the interfacial laboratory-derived flux laws (Chapter 4) are limited to 0.02–0.1 W m^{-2}. Of course, the accuracy of the 4/3 flux laws is debatable in the context of the observed staircases. It is unclear to what extent the extrapolation of the laboratory tank to the ocean is warranted – it is not unreasonable to expect an error

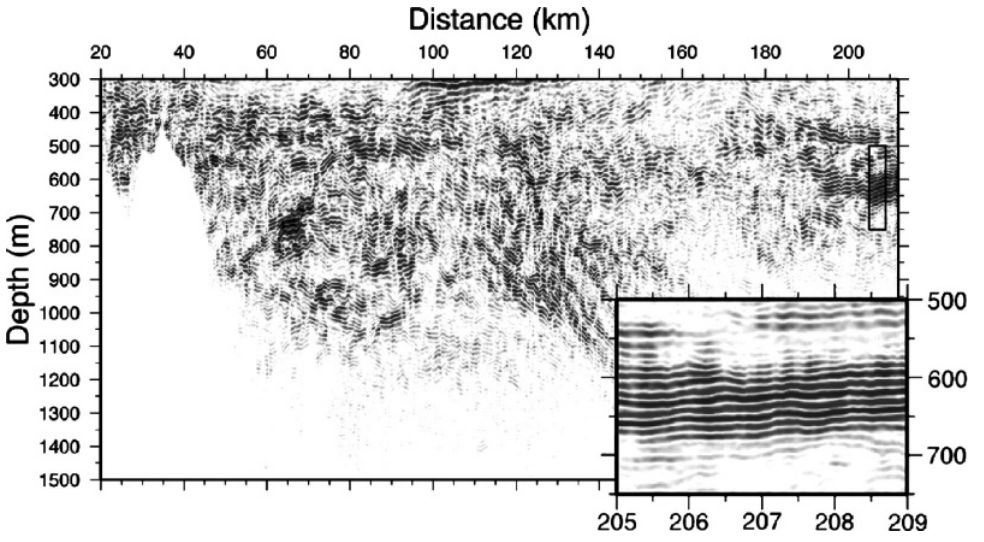

Figure 8.8 Seismic image of the Caribbean (C-SALT) staircase. From Fer *et al.*, (2010).

by a factor of two or more. Nevertheless, such estimates gave the oceanographic community a starting point for discussion of the potential contribution of staircases to the upper-ocean heat budget.

The data coverage of the upper Arctic in general, and our knowledge of staircase characteristics in particular, has improved dramatically since the commencement in 2004 of the Ice-Tethered Profiler (ITP) program, providing repeated sampling of the ice-covered upper-ocean Arctic (Toole *et al.*, 2011). The ITP program is currently active and more than fifty ITPs, distributed over much of the Arctic basin, have already been deployed. The number of observations provided by this program is impressive. The typical lifetime of an ITP is 500 days and each instrument produces on average 741 vertical profiles. Add to the picture their frequent sampling rate (two or more profiles per day) and vertical resolution of 25 cm, and it becomes clear that the ITPs are rapidly and dramatically increasing our knowledge of the Arctic stratification. Regarding the staircases, the first ITP-based results (e.g., Timmermans *et al.*, 2008) have already led to several firm and significant conclusions, of which we emphasize the following:

(i) Staircases are widespread throughout the central Arctic. Well-defined steps were absent in less than 4% of the ITP profiles. The smooth-gradient profiles were confined to selected regions, either located in close proximity to the basin boundaries or within strong mesoscale eddies.

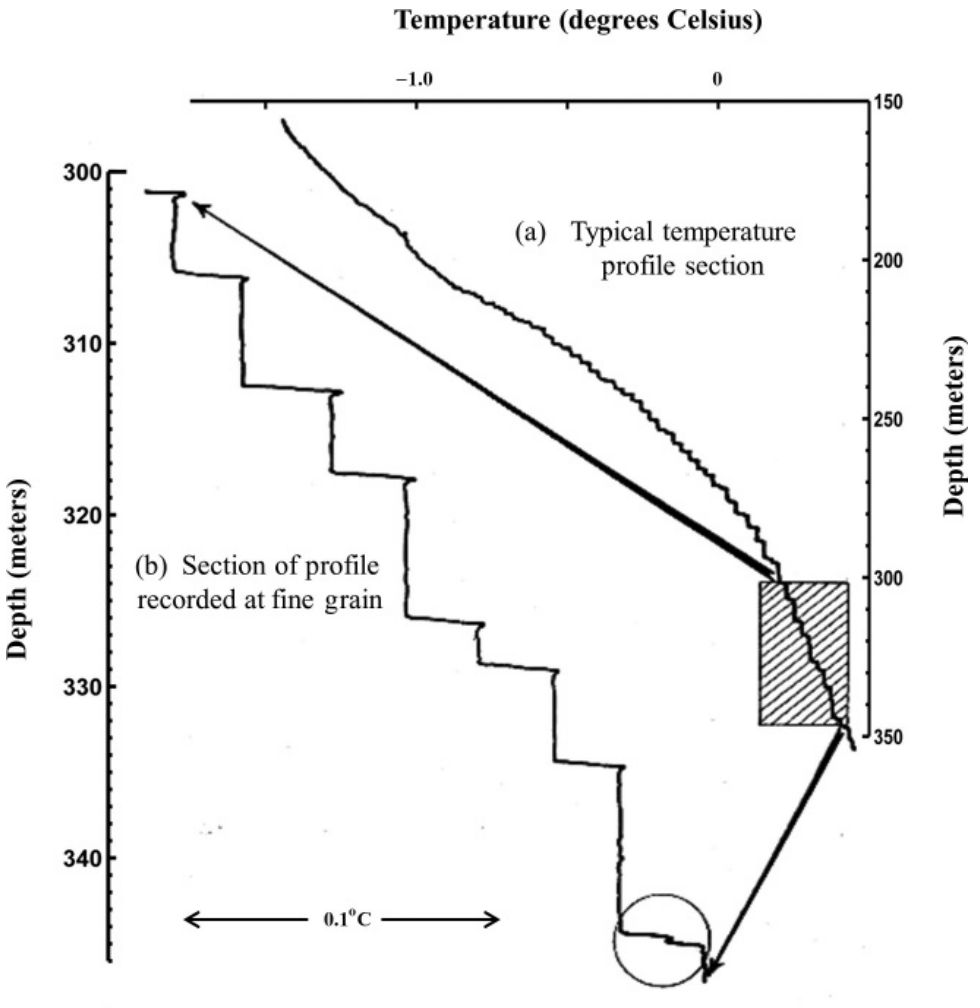

Figure 8.9 An example of temperature profile in the Arctic. From Neal *et al.* (1969).

(ii) Staircases are characterized by a remarkable spatial (hundreds of kilometers) and temporal (years) coherence. Most individual layers can be easily traced by their *T*–*S* values across the entire Beaufort Gyre and throughout the lifetime of each ITP.

(iii) Staircases actively respond to the climatic changes associated with warming and shoaling of the Atlantic Water. Relative to the AIWEX 1985 measurements, the present-day staircase region is approximately 100 m shallower and the thickness of steps is twice as large (~3 m average, with most steps in the 1–5 m range). The variation in temperature and salinities across typical

Table 8.1 *Characteristics of major staircases in the world ocean*

Location	Type	Density ratio	Step height	Temperature variation	Interfacial thickness	Buoyancy frequency (overall)
Western tropical Atlantic	SF	1.6	20 m	0.6 °C	2 m	$5 \cdot 10^{-3}$ s^{-1}
Tyrrhenian Sea	SF	1.2	400 m	0.2 °C	20 m	$4 \cdot 10^{-4}$ s^{-1}
Mediterranean outflow	SF	1.3	10 m	0.1 °C	1m	$2 \cdot 10^{-3}$ s^{-1}
Central Arctic	DC	4	3 m	0.05 °C	0.2 m	$4 \cdot 10^{-3}$ s^{-1}
Weddell Sea (upper)	DC	1.52	5 m	0.06 °C	0.1 m	$3 \cdot 10^{-3}$ s^{-1}
Weddell Sea (lower)	DC	1.36	80 m	0.13 °C	1 m	10^{-3} s^{-1}
Black Sea	DC	2	10 m (interior) 400 m (bottom)	0.05 °C	1 m	10^{-3} s^{-1}
Lake Kivu	DC	4	0.5 m	0.003 °C	0.2 m	$4 \cdot 10^{-3}$ s^{-1}

Salt finger and diffusive conditions are denoted as SF and DC respectively.
Thickness of the diffusive interfaces is based on the temperature stratification.

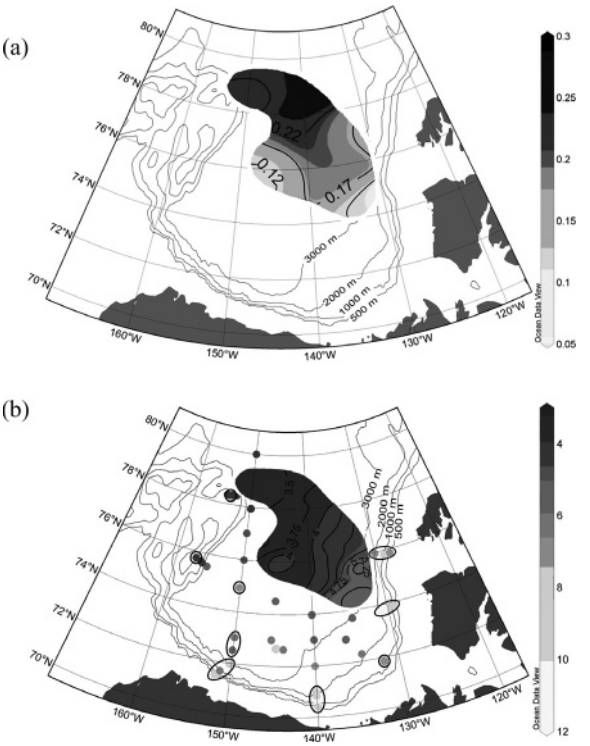

Figure 8.10 Distribution of the heat flux in W m^{-2} (a) and the average density ratio (b) in the diffusive layering region of the Beaufort Gyre estimated from the ITP data. From Timmermans *et al.* (2008). See color plates section.

interfaces are $\Delta T \approx 0.04$ °C and $\Delta S \approx 0.014$ – considerably higher than in the observations of Padman and Dillon (1987).

The distribution of the heat flux through staircases deduced from the 4/3 flux laws (Timmermans *et al.*, 2008) is shown in Figure 8.10a. The average value is $F_H \approx 0.22\,\mathrm{W\,m^{-2}}$, which exceeds earlier estimates (Padman and Dillon, 1987) by at least a factor of two. Figure 8.10b shows the distribution of (across-thermocline) density ratio in the Beaufort Gyre; values are limited to the range $2 < R_\rho^* < 7$ with the spatial average of $R_\rho^* \approx 4$. Layer-merging events have been observed but are rather rare, which suggests that the Arctic staircase is in a mature quasi-equilibrium state.

Figure 8.11 presents an example of a staircase from the Antarctic (Weddell Sea). Generally, Weddell staircases are characterized by much higher spatial and temporal variability. Muench *et al.* (1990) grouped the observed staircases into two distinct classes. Type A staircases are relatively shallow (limited to the upper 180 m) and small-scale (with step sizes of 1–5 m). Type B staircases are located in the

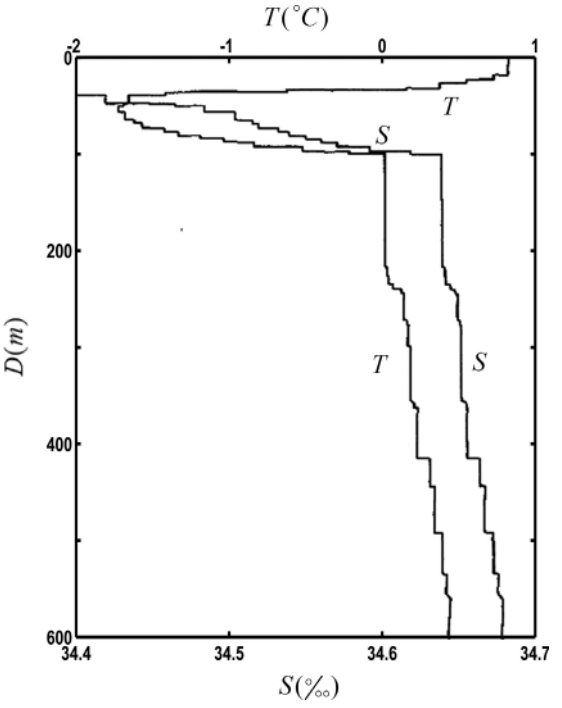

Figure 8.11 An example of the *T*–*S* profiles in the Weddell Sea (Antarctica). Note the distinct structure of steps in the upper and lower regions. From Foster and Carmack (1976).

weakly stratified portion of the thermocline (200–500 m) and vary considerably in step thickness (10–100 m). Robertson *et al*. (1995) examined data collected from a drifting ice station in the continental slope region of the western Weddell Sea. Their observations revealed the presence of small-scale (Type A) steps, statistics of which varied considerably over the observational period of three months in response to changes in the background stratification. The limited size of Type A steps could be associated with the temporal variability in the staircase, since significant periods of uninterrupted evolution are needed for the staircase to coarsen through a series of merging events. Deep (Type B) staircases, located in a more pristine environment, are likely to be closer to equilibration, which means thicker steps. Density ratio in the Weddell Sea is low ($R_\rho^* \sim 1.5$), which generally implies more active convection, thick steps and high *T*–*S* transport. Diffusively driven heat fluxes vary from $\sim$2 W m^{-2} in the slope region to $\sim$20 W m^{-2} in the interior, exceeding the Arctic fluxes by one to two orders of magnitude.

In addition to the Arctic and Antarctic examples, where diffusive layering is expected based on surface forcing patterns, diffusive staircases have also been

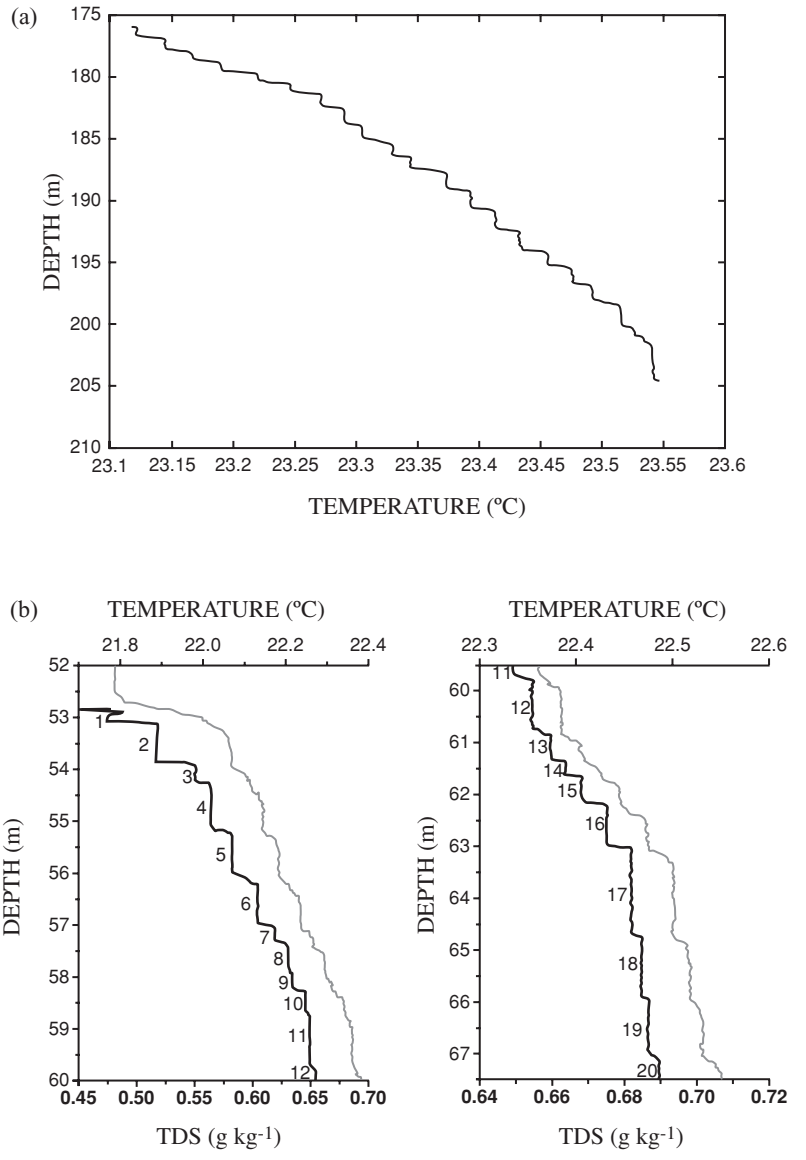

Figure 8.12 Typical temperature profiles taken in (a) Lake Kivu (from Newman, 1976) and (b) Lake Nyos (from Schmid *et al*., 2004).

observed in low- and mid-latitude regions, albeit on a much smaller scale. Interesting case studies include salt-water lakes. Figure 8.12 shows the temperature profiles taken in Lake Kivu (a) and Lake Nyos (b), which reveal characteristic staircase patterns with numerous small-scale but well-defined steps. The background stratification is predominantly diffusive, with heat at the bottom supplied by geothermal

springs. Great concern over the state of these lakes was caused by the catastrophic 1986 eruption of a carbon dioxide cloud in Lake Nyos, resulting in more than 1700 casualties, and fears that a similar disaster could happen in Lake Kivu. The Lake Nyos event stimulated a series of inquiries into the dynamics of vertical mixing. As is the case with many other diffusively stratified lakes, the water density in Kivu and Nyos is strongly affected, in addition to temperature and salinity, by several other components diffusing at different rates – carbon dioxide, methane and silica (Schmid *et al*., 2004, 2010). In such circumstances, the definition of the density ratio has to be broadened to incorporate the effects of all density components (Griffiths, 1979). Typical values of the modified density ratio ($R_\rho^* \sim 5$) suggest that both lakes are moderately susceptible to layering. However, in the absence of other significant sources of mixing, double-diffusion (or, to be more precise, multicomponent convection) dominates the vertical transport of heat, salt and dissolved gases.

Can we expect future catastrophic gas eruptions in these lakes? The reader can rest assured that it is highly unlikely. The degassing pipe installed in Lake Nyos effectively controls the recharging of carbon dioxide, keeping the lake in a safe state. For Lake Kivu, no such action is necessary. Diffusive mixing there is sufficient to remove the excess heat input into the deep water, without an equivalent upward transfer of dissolved salts and gases. The result is a stable self-regulating system, which guarantees the safety of people living in the vicinity of the lake (Schmid *et al*., 2010). Double-diffusion saves the day.

Diffusive staircases have been observed in several other locations. For instance, diffusive stratification of the Black Sea – a consequence of its prehistoric existence as a freshwater lake followed by the inflow of dense, warm and salty Mediterranean waters – supports irregular staircases in the upper part of the water column and the bottom convecting layer of ~450 m, maintained by the geothermal heat flux (Ozsoy *et al*., 1993). Diffusive layering is active in the deep layers of the Brazil–Malvinas Confluence zone, where it has been shown to control the vertical property fluxes (Bianchi *et al*., 2002). Pronounced staircases have been observed in the Antarctic Lake Vanda (Hoare, 1966, 1968; Huppert and Turner, 1972), in geothermal hot brine basins in the Red Sea (Turner, 1969; Anschutz and Blanc, 1996; Swift *et al*., 2012) and in the eastern Mediterranean (Boldrin and Rabitti, 1990).

Oceanographic measurements indicate that staircases are likely to form in diffusive stratification as long as the density ratio is in the range $1 < R_\rho^* < 10$. Occasionally, staircases have been observed for even larger values of R_ρ^*. Such a wide layering-favorable range is in contrast with the relatively restrictive conditions for salt-finger staircases, which require significant density compensation of temperature and salinity. In the diffusive case, the gradient of the (unstable) thermal density component needs to be only one-tenth of the corresponding (stable) haline

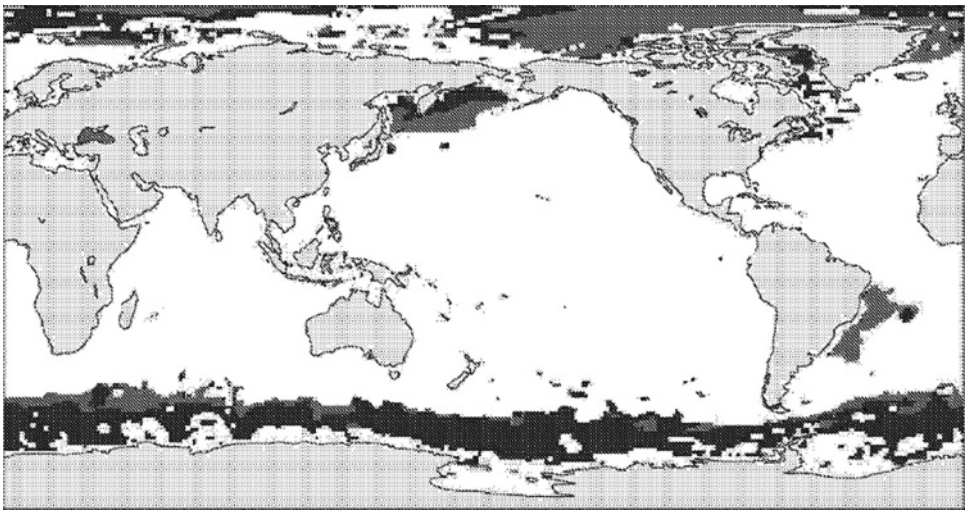

Figure 8.13 Ocean regions that are susceptible to diffusive layering. The light grey indicates areas with density ratios in the range $3 < R_\rho^* < 10$ somewhere in the water column and the dark grey indicates $1 < R_\rho^* < 3$. From Kelley *et al.* (2003).

gradient to produce well-defined staircases. Based on this criterion, it is possible to identify regions of the world ocean susceptible to diffusive layering, which are shown in Figure 8.13. As expected from the statistics of their incidence, diffusive staircase regions are mostly limited to the Arctic and Southern Oceans where, due to low temperatures, density stratification is often controlled by its haline component. In other susceptible areas, layering-favorable conditions are produced by region-specific interactions of distinct water masses.

8.2 Staircase origins

The list of usual explanations for the spontaneous formation of thermohaline staircases is a lengthy one. Staircase origin has been attributed to

(i) collective instability (Stern, 1969);
(ii) thermohaline intrusions that develop into a staircase (Merryfield, 2000);
(iii) metastable equilibria, initially forced by external disturbances (Stern and Turner, 1969);
(iv) applied flux mechanism (Turner and Stommel, 1964);
(v) negative density diffusion (Schmitt, 1994b);
(vi) instabilities of the flux-gradient laws followed by a series of mergers (Radko, 2003).

The overabundance of answers could be as disturbing as their absence. Much too often it is a warning sign that the proposed explanations are deficient in some respect and that the correct one has not been found. Fortunately, the situation with regard to the origin of staircases is not that bleak; we may be sufficiently close to establishing the leading contenders. Recent DNS of spontaneous layering have been particularly illuminating in this regard, although caution is certainly advised. To be objective, let us start by briefly reviewing the strengths and weaknesses of each hypothesis.

Collective instability mechanism

Perhaps the most influential hypothesis for the formation of staircases involves collective instability (Chapter 6). This idea was motivated by laboratory experiments in which staircases formed from the initially uniform *T*–*S* gradients (Stern and Turner, 1969). The appearance of layers was preceded by a period of active internal wave motion. Stern (1969) suggested that the growing wave might overturn and generate a stepped structure. Some support for this hypothesis comes from observations of oceanic staircases. Waves grow when the Stern number A exceeds unity (Chapter 6) and the measured values of A are indeed of order one in interfaces. However, there are several reasons to question the collective instability mechanism. For instance, in many laboratory experiments, salt and sugar replace heat and salt as buoyancy components and Stern numbers there are extremely low. Lambert and Demenkow (1972) report values as low as $A = 2 \cdot 10^{-3}$, casting doubt on the generality of Stern's (1969) criterion. Another dubious aspect is the assumed link between wave overturning and the formation of permanent well-defined staircases. Wave levels in regions of pronounced staircases (e.g., C-SALT area) are generally rather modest; numerous locations lacking staircases exist where waves are more active. At best, overturning internal waves produce transient irregular steppiness (Lazier, 1973; Lazier and Sandstrom, 1978) that is dynamically and structurally distinct from thermohaline staircases. Despite its undeniable historical interest, we cannot place the collective instability hypothesis too high on our list in terms of plausibility.

Thermohaline intrusion mechanism

The idea that staircases represent the final stage in the evolution of thermohaline intrusions is a relatively new one (Merryfield, 2000). As discussed in Chapter 7, intrusions can evolve either to a state consisting of alternating salt-finger and diffusive interfaces separated by convecting layers, which is common at high density ratio, or to a series of salt-finger interfaces when the density ratio is low

($R_\rho < 1.6$). The latter, argues Merryfield, form the observed oceanic staircases. This proposition is plausible, although it necessarily relies on the presence of lateral property gradients to drive interleaving. Intrusions-transformed-into-staircases are likely to exist in strong *T–S* fronts. For such regions, attempts have already been made to validate Merryfield's hypothesis using field measurements. Morell *et al.* (2006) analyzed a thermohaline staircase in a mesoscale eddy observed in the eastern Caribbean and found that the intrusion hypothesis is consistent with several aspects of the data. Intrusion-like structures, gradually morphing into regular steps, have been observed along the margins of the C-SALT staircase (Zhurbas and Ozmidov, 1983), suggesting that interleaving could play some role in the staircase dynamics.

The biggest question regarding the intrusion hypothesis concerns its generality. Can the intrusion mechanism explain the formation of major staircases, such as observed in the interior of the C-SALT area or Tyrrhenian Sea? Laboratory experiments (Stern and Turner, 1969; Krishnamurti, 2003) and numerical simulations (Radko, 2003; Stellmach *et al.*, 2011) indicate that staircases form spontaneously even in the absence of lateral gradients. Hence, intrusions are not essential for layering. For the intrusion hypothesis to be viable, we have to accept that the origins of the oceanic and laboratory/numerical staircases are fundamentally different. It is not impossible that two explanations are needed, one for the lab and another for the ocean, although most aspects of staircase experiments have proven to be highly suggestive of oceanographic observations.

Metastable equilibria mechanism

It has been speculated that staircases and smooth-gradient configurations represent distinct metastable equilibria. Stern and Turner (1969) suggested that finite amplitude perturbations to the gradient state force the system into a layered regime where it can remain for long periods of time (even indefinitely if the overall variation in temperature and salinity is maintained). In retrospect, it is clear that this mechanism does play some role in the evolution of staircases. Large initial perturbations to the gradient state undoubtedly make the transition to the staircase more likely and expedite the process. Once the staircase is created, the system becomes resilient to further structural changes. In this regard, Stern and Turner's insight is truly impressive, particularly considering that it was based on very early and qualitative laboratory experiments. The ability of sufficiently strong perturbations to transform the smooth gradient into a dramatically distinct state is linked to the subcritical nature of layering instabilities. In subcritical instabilities, nonlinearity tends to destabilize the system, leading to a harder transition to a new regime and also making this transition dependent on the initial perturbation amplitude.

The big question with regard to the metastable equilibria hypothesis is whether the finite amplitude perturbations are necessary for the spontaneous formation of layered states. For the diffusive case, the answer is yes. Calculations by Veronis (1965, 1968) – albeit performed in the context of the bounded model (Chapter 5) – have shown that when the uniform-gradient solution is linearly stable, finite amplitude perturbations can drive the system into a steady nonlinear convecting regime and often do so. For salt-finger staircases, however, the emerging evidence suggests that under typical conditions ($R_\rho < 2$) the uniform-gradient solution is *linearly* unstable. Numerical simulations (Radko, 2003; Stellmach *et al*., 2011), laboratory experiments (Krishnamurti, 2003) and analytical arguments (Radko, 2003) indicate that layering can be initiated by small-amplitude perturbations. The layering instability takes the form of horizontally homogeneous modes that ultimately transform smooth stratification into well-defined steps. Thus, the metastable equilibria mechanism is not essential for finger-induced layering and plays only an auxiliary role in the transition to staircases.

Applied flux mechanism

A somewhat special mechanism of layering is realized in laboratory experiments in which a stable salinity gradient is heated from below (Turner and Stommel, 1964; Huppert and Linden, 1979). The direct response to the applied heat flux is top-heavy convection in the lower part of the water column. The convecting layer is well mixed and bounded from above by a thin high-gradient interface, which is clearly visible in vertical temperature profiles taken during the experiment (Fig. 8.14). Heat is transferred upward from the convecting layer by a combination of molecular diffusion and entrainment across the interface. Since the molecular transfer of heat exceeds that of salt, the net result is the supply of buoyancy to the region immediately above the interface, which leads to the formation of a second convecting layer. The process then repeats over and over, resulting in a sequence of mixed layers separated by sharp interfaces – the thermohaline staircase.

The basic dynamics of layering in the bottom-heated case are robust and well understood. Similar processes are expected to occur when the diffusive stratification is cooled from above (Molemaker and Dijkstra, 1997) and when the salt flux is applied at the top of the salt-finger favorable stratification. It is, however, unclear whether the prescribed flux boundary condition is appropriate for oceanic layering. The applied flux mechanism is most likely at work in cases when layering is caused by geothermal heating, examples of which were given in the previous section. The dynamics of the more prominent staircases – such as observed in the

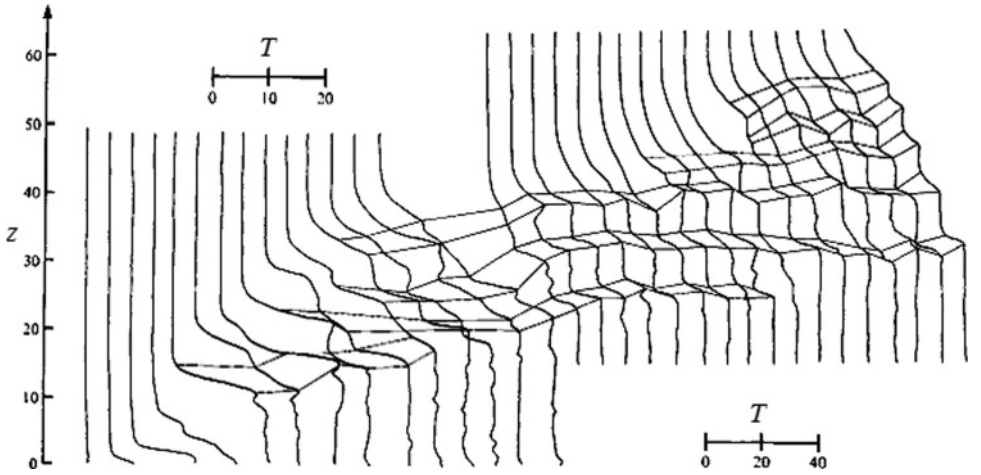

Figure 8.14 A set of temperature–depth profiles taken during the course of a laboratory experiment in which a stable salinity gradient is heated from below. Each successive profile is offset to the right. From Huppert and Linden (1979).

Arctic or in the C-SALT area – are substantially different. The layering-favorable conditions there result from the juxtaposition of distinct water masses rather than from the surface/bottom buoyancy forcing. In such cases, causality is reversed: layering is no longer controlled by the fluxes but, rather, fluxes are determined by the pattern of stratification. Numerical simulations of layering in the effectively unbounded gradients tend to confirm the subservient role of fluxes. As layers form and sequentially merge, the vertical transport of heat and salt dramatically increases.

Negative density diffusion

To explain the mechanism of layering, oceanographers often point out that if the flux of density is counter-gradient, it should have a destabilizing effect on smoothly stratified regions of the ocean (Schmitt, 1994b). The origin of this idea can be traced to the heuristic arguments put forward by Phillips (1972) and Posmentier (1977) for one-component turbulent fluids. At first glance, this explanation comes across as an even better fit to the thermohaline layering problem. Double-diffusion is driven by the release of potential energy of the background stratification; the light upper part of the water column becomes lighter, the heavy lower part becomes even heavier. Hence, the eddy diffusivity of density is negative, which by itself implies the instability of a uniform gradient and a likely transition to a different stratification pattern.

The negative diffusion argument can be made more quantitative by focusing on the one-dimensional diffusion equation of density:

$$\frac{\partial \rho}{\partial t} = \frac{\partial}{\partial z}\left(K_\rho \frac{\partial \rho}{\partial z}\right). \tag{8.5}$$

Suppose for a moment that the eddy diffusivity is uniform and negative ($K_\rho = const < 0$). Perturbing the uniform background stratification ($\bar{\rho}_z = const$) by a small-amplitude normal mode $\rho' = \hat{\rho}\exp(imz + \lambda t)$ yields the growth rate equation:

$$\lambda = -K_\rho m^2 > 0. \tag{8.6}$$

The positive growth rates imply the instability of the basic state, which can lead to layering. One of the technical difficulties with this formulation is related to the ill-posedness of the negative diffusivity model: the growth rate increases without bound with the wavenumber (m). This problem, however, is not fundamental. The concept of eddy diffusivity assumes some scale separation between eddies and the mean field, and the ultraviolet catastrophe in the negative diffusivity model can be prevented by applying (8.5) only to scales substantially exceeding the salt-finger width.

Unfortunately, the negative diffusivity model suffers from at least two other inconsistencies that severely limit its ability to explain the mechanism of layering. First, (8.6) implies that the uniform gradient is always unstable and therefore transition to staircases is expected regardless of the specific conditions. This conclusion is obviously false. The oceanic heat–salt staircases form in a relatively narrow range of density ratios $1 < R_\rho < 2$ – only 1% of the net salt-finger favorable range $1 < R_\rho < \tau^{-1} \approx 100$. Call me a pessimist, but if a model gives a wrong answer in 99% of cases, it must be missing some essential physics. Doubts as to its relevance linger even when the model does make a correct prediction for low density ratios.

The second problem with regard to the negative diffusivity mechanism is related to the strong dependence of diffusivity on the density ratio. In double-diffusive convection, the mixing intensity rapidly diminishes with increasing R_ρ, the significance of which becomes apparent when (8.5) is rewritten as

$$\frac{\partial \rho}{\partial t} = K_\rho \frac{\partial^2 \rho}{\partial z^2} + \frac{\partial K_\rho}{\partial R_\rho}\frac{\partial R_\rho}{\partial z}\frac{\partial \rho}{\partial z}. \tag{8.7}$$

While the first term on the right-hand side of (8.7) is always destabilizing, it is usually less than the second (stabilizing) term. The layering conditions are ultimately controlled by the competition between the "negative diffusivity" and "variable diffusivity" mechanisms. Thus, the negative diffusivity hypothesis in its original form ignores a very significant aspect of the layering problem. To

summarize, the negative diffusivity view may have some merit, but only in a very general and qualitative sense. Any meaningful quantitative model of double-diffusive layering should necessarily take into account the dependence of mixing characteristics on the density ratio.

My money is on the sixth and final hypothesis considered here – the instability of flux-gradient laws – which builds on the negative diffusivity model but puts it on a more solid and physical footing. Instead of combining temperature and salinity into a single density term, it follows a more natural, for double-diffusive problems, approach and treats both density components individually. The flux law instability mechanism does not seem to suffer from inconsistencies that plague other theories of double-diffusive layering and it has been successfully tested by DNS. These features warrant a more detailed discussion of the flux law hypothesis, which follows next.

8.3 Instability of the flux-gradient laws

To be specific, we discuss the flux law instability in the context of salt-finger favorable stratification, which has been favored for several reasons (including traditional preference) by most theoretical studies of layering. It should be understood, however, that the following model can be readily adapted for the diffusive regime as well, provided the background stratification is susceptible to the primary oscillatory instability. Consider the one-dimensional (z) large-scale temperature and salinity equations

$$\begin{cases} \dfrac{\partial T}{\partial t} = -\dfrac{\partial}{\partial z} F_T, \\ \dfrac{\partial S}{\partial t} = -\dfrac{\partial}{\partial z} F_S, \end{cases} \tag{8.8}$$

which, in essence, represent the two-component counterpart of (8.5). F_T and F_S are the vertical temperature and salinity fluxes that we attribute to salt fingering. All variables are non-dimensionalized using the standard system (1.11), which makes it possible to express the fluxes in terms of the Nusselt number and flux ratio as in (6.3).

The next step involves the development of a mixing model. Following the treatments of collective instability in Chapter 6 and thermohaline interleaving in Chapter 7, we assume that both the Nusselt number (Nu) and the flux ratio (γ) are uniquely determined by the local density ratio (R_ρ) and (8.8) is linearized with respect to the uniform background gradients. The linear perturbations of

temperature and salinity fluxes are given in (6.5)–(6.7), which reduce the governing system (8.8) to

$$\begin{cases} \dfrac{\partial T'}{\partial t} = A_{Nu}\dfrac{\partial^2}{\partial z^2}\left(T' - \bar{R}_\rho S'\right) + Nu(\bar{R}_\rho)\dfrac{\partial^2 T'}{\partial z^2}, \\ \dfrac{\partial S'}{\partial t} = A_\gamma Nu(\bar{R}_\rho)\dfrac{\partial^2}{\partial z^2}\left(T' - \bar{R}_\rho S'\right) + \gamma^{-1}(\bar{R}_\rho)\dfrac{\partial T'}{\partial t}, \end{cases} \tag{8.9}$$

where $\bar{R}_\rho$ is the basic density ratio and $A_{Nu} = \bar{R}_\rho \left.\frac{\partial Nu}{\partial R_\rho}\right|_{R_\rho=\bar{R}_\rho}$ and $A_\gamma = \bar{R}_\rho \left.\frac{\partial \gamma^{-1}}{\partial R_\rho}\right|_{R_\rho=\bar{R}_\rho}$. Stability properties of the resulting linear system are analyzed using the normal modes

$$\begin{pmatrix} T' \\ S' \end{pmatrix} = \begin{pmatrix} \hat{T} \\ \hat{S} \end{pmatrix} \exp(imz + \lambda t). \tag{8.10}$$

When (8.10) is substituted in the linear system (8.9) and $\left(\hat{T}, \hat{S}\right)$ are eliminated, we arrive at the quadratic eigenvalue equation for the growth rate λ:

$$\lambda^2 + \lambda\left(A_{Nu} + Nu(\bar{R}_\rho) - A_\gamma Nu(\bar{R}_\rho)\bar{R}_\rho - \frac{\bar{R}_\rho A_{Nu}}{\gamma(\bar{R}_\rho)}\right)m^2 - A_\gamma Nu^2(\bar{R}_\rho)\bar{R}_\rho m^4 = 0. \tag{8.11}$$

The stability/instability of the system is determined by the coefficients of Eq. (8.11) and, ultimately, by the background density ratio $\bar{R}_\rho$. Of particular significance is the sign of A_γ. Theoretical arguments and numerical simulations (Chapter 2) indicate that the $\gamma(R_\rho)$ dependence is non-monotonic. As the density ratio increases from unity, the flux ratio first decreases, as shown in Figure 8.15, reaches a minimum value ($R_{\min}$) and then starts to increase. For density ratios in the range $1 < \bar{R}_\rho < R_{\min}$, the free coefficient of the quadratic equation (8.11) is negative ($A_\gamma > 0$), which implies that there are two real roots of opposite sign. The existence of a positive root means that the basic uniform gradient is unstable. It can also be shown that, under certain unrestrictive assumptions, the flux-gradient laws are stable for $\bar{R}_\rho > R_{\min}$. Thus, the decrease of γ with R_ρ is both a necessary and sufficient instability condition. This instability can be thought of as a special one-dimensional case of the intrusive γ-instability modes discussed in Chapter 7.

Analysis of the amplitude/phase relationships for T', S', R_ρ and γ in a growing normal mode suggests the following physical explanation of layering. If the amplitude of the temperature perturbation ($\hat{T}$) exceeds the amplitude of the salt perturbation ($\hat{S}$), as shown in a schematic in Figure 8.16, then the density ratio R_ρ reaches its maximum at the location of the largest temperature gradient (that is, $z = 0, 2\pi/m$ in Fig. 8.16). If γ were constant, then the growth rate of the first normal mode in (8.11) would be zero – T and S would not change in time, which means

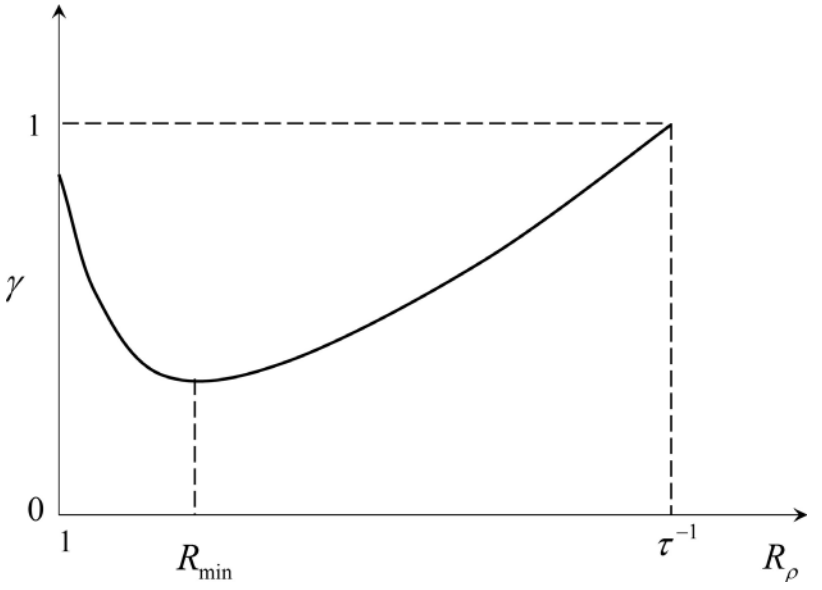

Figure 8.15 Dependence of the flux ratio on the density ratio.

that F_T and F_S are uniform in z. However, when γ is a decreasing function of R_ρ, there is an increase of the heat/salt flux ratio at $z = \pi/m$ and, correspondingly, a decrease at $z = 0, 2\pi/m$. As a result, the temperature flux convergence at $0 < z < \pi/m$ (and divergence at $\pi/m < z < 2\pi/m$) exceeds that for salt. This convergence pattern leads to an enhanced accumulation of heat, relative to the accumulation of salt, in the lower part of the layer in Figure 8.16. This, in turn, is followed by an additional increase in R_ρ at $z = 0, 2\pi/m$ and, correspondingly, further decreases γ there. At $z = \pi/m$, the density ratio further decreases while the flux ratio increases. This self-enhancing mechanism produces a monotonic growth of the perturbation.

It is easy to imagine how the γ-instability can transform a smooth T–S gradient into a staircase. Suppose that the growth of the unstable horizontally uniform modes persists long enough for the fluid to develop density reversals, as indicated in the schematic in Figure 8.17. These top-heavy regions overturn and the fingering interfaces become sandwiched between nearly homogeneous convecting layers. Since the finger-driven flux of density across the interfaces is up-gradient (downward), there is a continuous supply of density to the top of each convecting layer; density is removed at the bottom. This forcing pattern maintains convection in mixed layers. Vigorous convection in layers, in turn, prevents salt-finger zones from spreading vertically and the system remains locked in the staircase regime.

Conditions for the γ-instability are generally consistent with the incidences of layering in the ocean. The pattern of $\gamma(R_\rho)$ for the oceanic (heat/salt) parameters

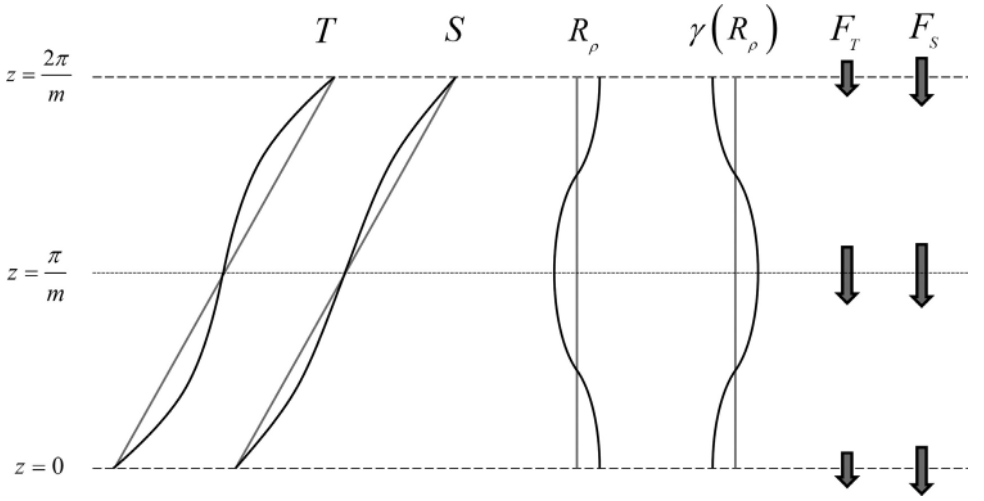

Figure 8.16 Schematic diagram illustrating the physical mechanism of the γ-instability. Decrease in γ with R_ρ results in the growth of the perturbations on a uniform $T-S$ gradient (see the text). After Radko (2003).

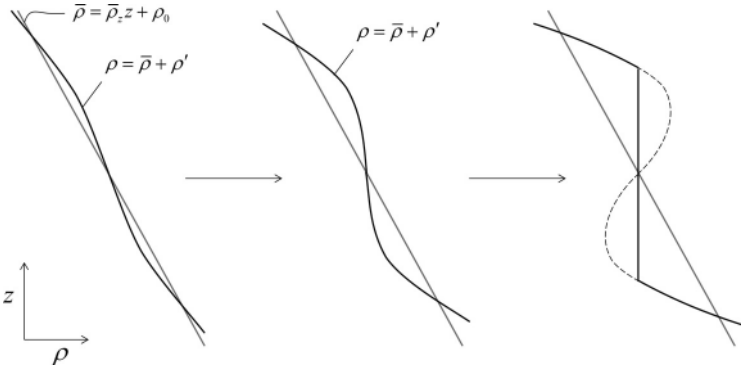

Figure 8.17 Transition from the smooth-gradient to staircase configuration. The growing horizontally uniform perturbation develops top-heavy regions that rapidly overturn, producing mixed layers separated by high-gradient interfaces.

(Fig. 2.7a) is such that the most significant decrease in γ occurs within the interval $1 < R_\rho < 2$, which rationalizes both observations of staircases for low R_ρ and the lack of staircases for $R_\rho > 2$. Another consideration for the ocean involves the contribution of turbulent mixing by overturning gravity waves. Turbulence tends to mix temperature and salinity at equal rates and therefore $\gamma_{\text{turb}} = R_\rho$. Taking into account this contribution shifts the minimum of the net flux ratio towards lower density ratios. The magnitude of this shift is as uncertain as our knowledge of turbulent diffusivity in the thermocline. However, it is not unreasonable to assume

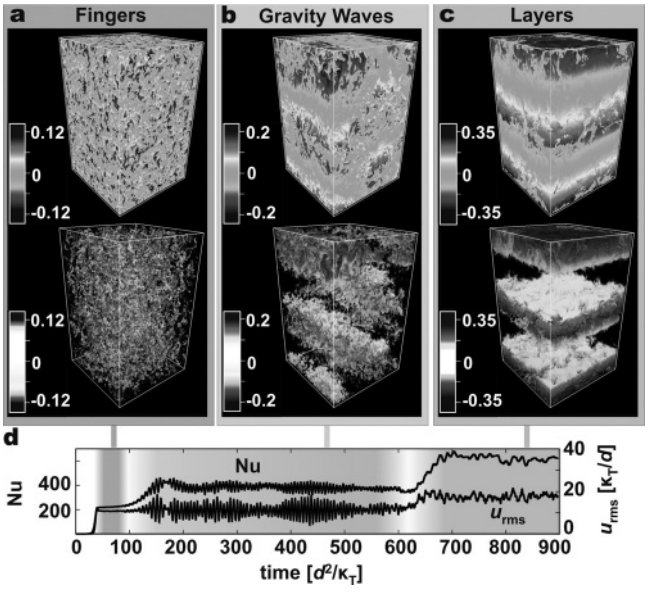

Figure 8.18 Simulated layer formation in a large triply periodic domain. Temperature perturbations are shown in color, with their respective color scales in each panel. The top panels are visualizations on the data-cube faces, while the lower ones are volume-rendered images. Snapshots are shown for three characteristic dynamical phases: (a) homogeneous fingering convection, (b) flow pattern dominated by gravity waves, (c) formation of vigorously convecting layers separated by thin fingering interfaces. (d) Time series of the Nusselt number and the flux ratio. From Stellmach *et al*. (2011). See color plates section.

that the minimum of the $\gamma(R_\rho)$ relation for the combination of double-diffusion and turbulence matches the typical point of staircase/gradient transition in observations ($R_{\min} \approx 1.7$).

Diagnostics of spontaneous layering in DNS – both two-dimensional (Radko, 2003) and three-dimensional (Stellmach *et al*., 2011) – confirm that layering is indeed driven by the γ-instability. Figure 8.18 shows a sequence of events leading to staircase formation. The experiment was initiated by a uniform salt-finger favorable gradient. The vigorous field of salt fingers emerges very rapidly (Fig. 8.18a) and initially lacks any signs of large-scale self-organization. However, this homogeneous fingering state does not persist for long. The next evolutionary phase is defined by the presence of an internal wave field, which is a direct and expected consequence of the collective instability (Chapter 6). Waves grow until their amplitude is sufficiently large to develop intermittent density overturns. After saturation, the system remains in the wave-dominated state for a substantial period of time ($150 < t < 600$ in standard non-dimensional units). At this stage, the wave

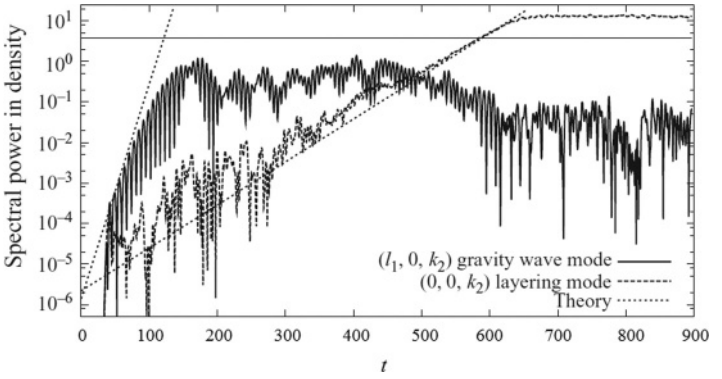

Figure 8.19 Diagnostics of the numerical simulation in Figure 8.18. Shown is the temporal evolution of the dominant gravity-wave mode and of the γ-mode ultimately producing the staircase along with the predictions based on the parametric theory. While the gravity-wave mode rapidly saturates, the γ-mode slowly but steadily grows up to the critical amplitude for overturning (indicated by the horizontal line). From Stellmach *et al*. (2011).

activity is visually most striking (Fig. 8.18b). After observing waves of such magnitude it is easy to appreciate why the early explanations of layering ascribed critical significance to collective instability (Stern and Turner, 1969). In reality, the role of waves is surprisingly limited. The spatially averaged *T*–*S* fluxes, expressed in terms of Nusselt number and flux ratio in Figure 8.18d, are modulated by waves. However, their time-mean values remain largely unchanged until the system enters the third phase – the emergence of a staircase (Fig. 8.18c).

The two-layer structure in Figure 8.18c is produced by slow but persistent growth of the horizontally uniform Fourier mode with the vertical wavelength of half the domain size. Eventually, this mode generates density inversions, which overturn and produce well-mixed convecting layers, in accord with the scenario depicted in Figure 8.17. A time record of the amplitude of the layering mode (diagnosed from the DNS) is plotted along with the theoretical prediction based on Eq. (8.11) in Figure 8.19; their apparent agreement confirms the relevance and accuracy of the parametric model. It is also instructive to compare the evolutionary patterns of layers and waves in the DNS experiment. The most energetic wave mode, also shown in Figure 8.19, grows more rapidly than the layering mode and reaches saturation much faster. However, even when the wave activity is maximal, it does not significantly affect the layering mode, which continues to grow at the predicted rate until the staircase is formed. Waves are far more fragile. Upon reaching the near-saturation amplitude, the layering mode substantially suppresses the wave motion.

The experiment in Figure 8.18 shows that, overall, waves do little in the layering process – despite spectacular amplitudes, they control neither small-scale mixing by salt fingers nor the growth of the large-scale layering modes. In this regard, it should be acknowledged with sadness that the literature on double-diffusion (or on any exciting topic for that matter) is often polluted with myths and unsubstantiated conclusions. One of the most widespread notions is that the vertical shear induced by internal waves in the ocean has a devastating effect on fingers and on secondary double-diffusive structures. Numerical simulations, such as the DNS reported by Stellmach *et al.* (2011), demonstrate that this notion is without basis.

The final question we wish to discuss in this section concerns the preferred vertical scale of layering modes. Analysis of the growth rate equation (8.11) for the unstable regime ($R_\rho < R_{\min}$) shows that its positive root scales as

$$\lambda_1 \sim -\frac{\partial \gamma}{\partial R_\rho} Nu\ m^2. \tag{8.12}$$

Equation (8.12) implies that the growth rate increases without bound with the perturbation wavenumber (m) and therefore the model suffers from the ultraviolet catastrophe (similar to that in the negative diffusivity model discussed in Section 8.2). This brings in a couple of related complications. The first one is that the model becomes obviously unphysical if the prediction in (8.12) is taken literally – infinitely large growth rates are prohibited in nature.

This criticism is relatively easy to dismiss by simply recalling that the theory assumed from the outset a certain scale separation between large-scale layering modes and salt fingers. The model in general and (8.12) in particular applies only to sufficiently small wavenumbers ($m < m_0$). The range of validity cannot be deduced internally from the theory. However, simulations (Traxler *et al.*, 2011a; Stellmach *et al.*, 2011) indicate that scales exceeding the salt-finger width by an order of magnitude or more are accurately represented by the model; smaller scales are not. Thus, the largest growth rates are expected to occur in the vicinity of the point of failure of the theoretical model $m_0 \sim 0.1 \cdot k_f$, where k_f is the typical horizontal wavenumber of salt fingers. The calculation in Figure 8.18 corroborates this suggestion: the wavelength of the γ-instability mode (L_γ) destined to evolve into the staircase exceeds the fastest growing finger width by a factor of twenty. In dimensional units, evaluated for typical stratification of the mid-latitude thermocline, this translates to

$$L_\gamma \sim 1 - 2\,\mathrm{m}. \tag{8.13}$$

The estimate (8.13) is a cause for concern. The limited scale of layering instability seems to be at odds with oceanographic observations of much thicker steps

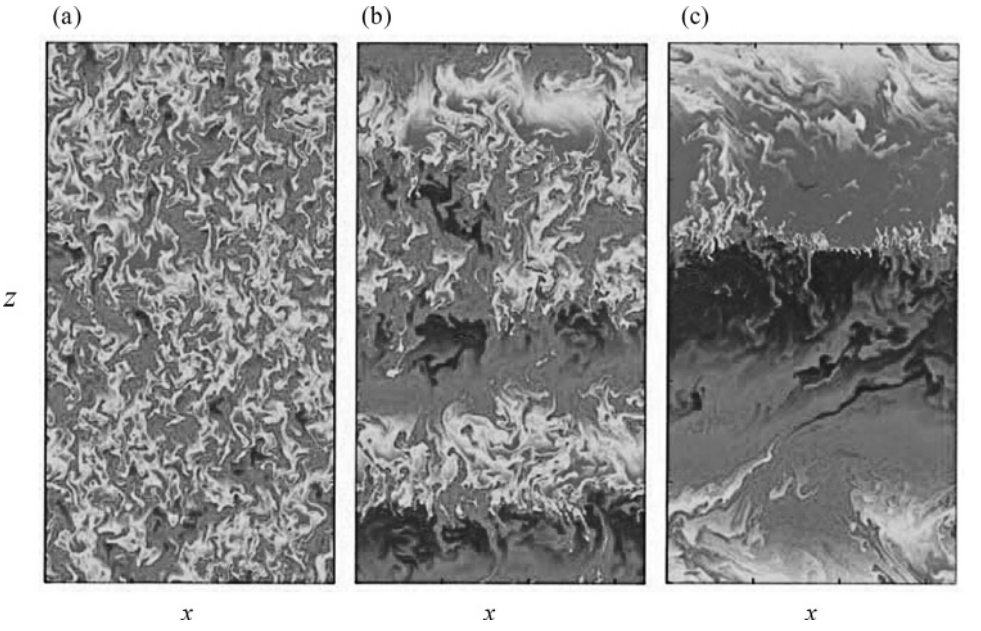

Figure 8.20 Formation and evolution of layers in a numerical experiment. Instantaneous perturbation temperature fields are shown for (a) $t = 50$, (b) $t = 400$ and (c) $t = 800$ (standard non-dimensional units). Note the spontaneous appearance of layers, followed by their systematic mergers. From Radko (2003). See color plates section.

of 10–100 m, which are more common in salt-finger staircases. Fortunately, numerical simulations offer an important hint for the step-size selection puzzle. Figure 8.20 shows the formation and evolution of layers in a two-dimensional DNS (Radko, 2003). As expected, the layers that formed first are relatively thin ($\sim$10–20 times the finger wavelength). However, in time they merge sequentially until there is only one interface left within the limits of the computational domain. Profiles of the horizontally averaged density (Fig. 8.21) reveal a general tendency for strong steps characterized by significant temperature and salinity jumps to grow further at the expense of weaker steps, which gradually erode and eventually disappear. This merging pattern – referred to as the "*B*-merger" mode in Radko's (2007) classification (Section 8.4) – is reminiscent of the evolution of the Tyrrhenian Sea staircase in Figure 8.6. Sequential layer mergers have also been observed in the laboratory experiments on the spontaneous gradient/staircase transition (Krishnamurti, 2003). Figure 8.22 presents the layering simulation in the diffusive regime (Prikasky, 2007). The evolutionary pattern of steps is strikingly similar to that of salt-finger staircases (Fig. 8.20). Layers that develop initially are not steady but merge continuously and the characteristic step size increases substantially.

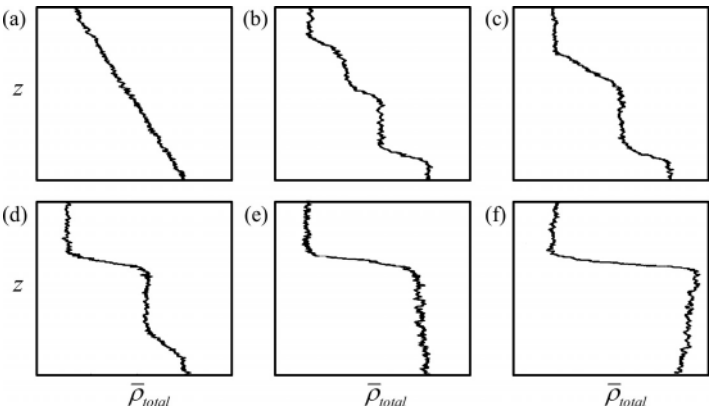

Figure 8.21 Evolution of the horizontally averaged density for the calculation in Figure 8.20. From Radko (2003).

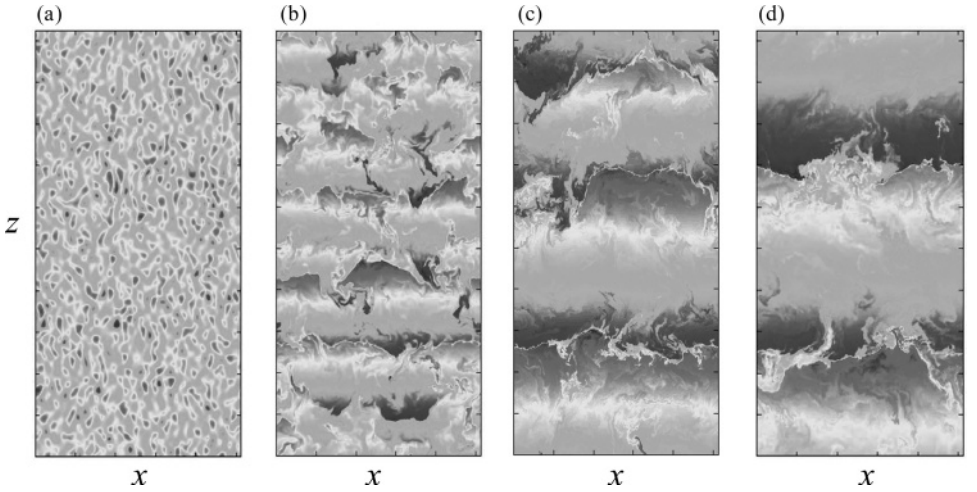

Figure 8.22 Direct numerical simulations of spontaneous layering from the uniform gradient in a diffusively stratified fluid. The small-scale oscillatory perturbations give way to horizontally uniform layers, which merge sequentially until producing the final quasi-equilibrium state. From Prikasky (2007). See color plates section.

If the merging scenario is commonly realized in oceanic staircases, then the initial thickness of layers is of secondary importance. Nature has all the time it needs to complete the transition to the ultimate equilibrium state. In this case, the observed step size is controlled by processes that arrest the coarsening of a staircase and the final thickness of layers can greatly exceed the initial one. Regarding the equilibrium step size, it should be mentioned that some general conclusions

could be reached on the basis of dimensional analysis, without even formulating a mechanistic model of staircase evolution. If no length scale is imposed externally, then the non-dimensional step height is uniquely determined by the density ratio, which can be expressed in dimensional units as follows:

$$H_{\text{dim}} = \left(\frac{k_T \nu}{g\alpha \bar{T}_z}\right)^{\frac{1}{4}} H(R_\rho). \tag{8.14}$$

Alternatively, (8.14) can be written in terms of the buoyancy frequency (N):

$$H_{\text{dim}} = \left(\frac{k_T}{N}\right)^{\frac{1}{2}} G(R_\rho), \tag{8.15}$$

where $G = H\left[Pr(1 - R_\rho^{-1})\right]^{\frac{1}{4}}$. Kelley (1984) and Kelley *et al*. (2003) used various oceanographic observations of diffusive staircases to demonstrate that (8.15) captures the general trend of step-size distribution. The departures of data from (8.15) are noticeable but can be attributed to an incomplete equilibration of some staircases examined by Kelley *et al*. While it is reassuring that dimensional analysis can predict gross features of staircases, deeper insight into fluid dynamical phenomena usually requires development of explicit physical models. Some results in this direction, based on layer-merging theory, are discussed next.

8.4 Mechanics of layer-merging events

The first ideas on the evolution of staircases were introduced by Huppert (1971). The essential insight from his model is that the dynamics of layers should be treated as a secondary instability problem. A series of identical steps might well be an exact steady solution of the governing equations, but whether or not the system will remain in this state depends on its stability. Huppert's theory, originally formulated for diffusive staircases, is now adapted for the salt-finger case and, for pedagogical reasons, expressed in terms of the simplest system consisting of two layers.

Consider the configuration shown in Figure 8.23. Figure 8.23a represents a basic state consisting of a series of identical thin salt-finger interfaces separated by convecting layers of equal thickness H. This steady state is perturbed as indicated in Figure 8.23b: we increase slightly the T–S jump at the interface $z = z_1$, but decrease the jump at the adjacent interfaces. The vertical structure is assumed to be periodic with the z-wavelength of $2H$. This state can be thought of as an infinite series of layers in which we simultaneously reduce the magnitude of temperature and salinity jumps (ΔT, ΔS) at all steps with even numbers and correspondingly increase the jumps across the odd steps. Note that such a perturbation does not affect

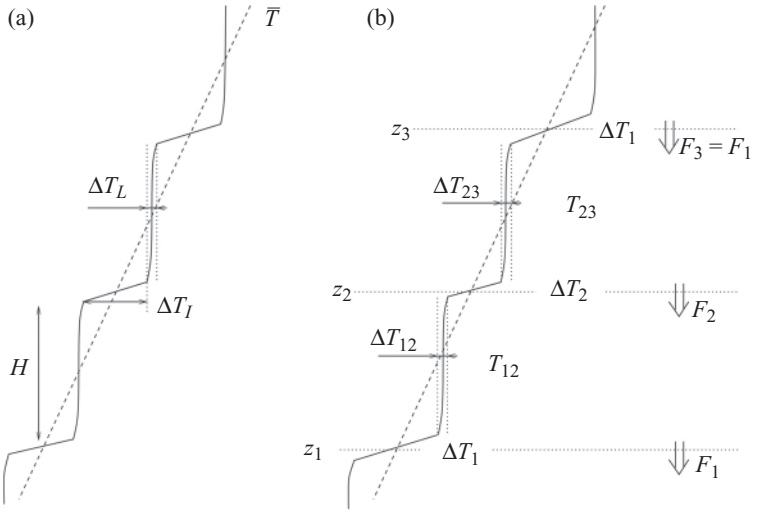

Figure 8.23 Schematic diagram illustrating the stability analysis for an infinite series of interfaces. (a) Basic state consisting of identical steps. (b) Perturbed state in which the *T*–*S* jumps at the even interfaces are slightly decreased, and the jumps at odd interfaces are increased. From Radko (2005).

the overall *T*–*S* gradient. Our objective is to determine whether the disturbance will grow in time, implying instability of the basic state in Figure 8.23a, or remain small.

The most basic version of the model (Huppert, 1971; Radko, 2003) invokes the following simplifying assumptions:

(i) the temperature and salinity variations across the convecting layers $(\Delta T_L, \Delta S_L)$ are not taken into account;
(ii) fluxes across the interfaces are parameterized using the 4/3 flux law $F_T = C(R_\rho)\Delta T^{\frac{4}{3}}$, $F_S = \frac{F_T}{\gamma(R_\rho)}$;
(iii) the vertical drift of the interfaces is ignored.

The amplitude of the merging perturbation in Figure 8.23 is conveniently represented by quantities $A = \frac{\Delta T_2 - \Delta T_1}{\Delta T_I}$ and $B = \frac{\Delta S_2 - \Delta S_1}{\Delta S_I}$ – the relative variations in the interfacial jumps of temperature and salinity The heat and salt budgets for each mixed layer are then expressed in terms of A and B, the result is linearized, and the stability of the system is analyzed using the normal modes $(A, B) = (A_0, B_0)\exp(\lambda t)$. The resulting growth rate equation takes the

following form:

$$\lambda^2 + \frac{4(\bar{T}_z)^{\frac{1}{3}}}{H^{\frac{2}{3}}}\left[\frac{4}{3}C(\bar{R}_\rho) + A_C - \frac{\bar{R}_\rho A_C}{\gamma(\bar{R}_\rho)} - A_\gamma C(\bar{R}_\rho)\bar{R}_\rho\right]\lambda - \frac{16}{3}\frac{4(\bar{T}_z)^{\frac{2}{3}}}{H^{\frac{4}{3}}}C^2(\bar{R}_\rho)\bar{R}_\rho A_\gamma = 0, \tag{8.16}$$

where $A_C = \bar{R}_\rho \left.\frac{\partial C}{\partial R_\rho}\right|_{R_\rho=\bar{R}_\rho}$ and $A_\gamma = \bar{R}_\rho \left.\frac{\partial \gamma^{-1}}{\partial R_\rho}\right|_{R_\rho=\bar{R}_\rho}$.

Equation (8.16) is structurally analogous to the growth rate equation for the layering instability (8.11) and the stability conditions set by these equations are also very similar – everything is controlled by the sign of A_γ. If the flux ratio (γ) decreases with increasing R_ρ, as expected for low density ratios (see Fig. 8.15) then $A_\gamma > 0$ and the free coefficient of the quadratic equation (8.16) is negative, which implies two real roots of opposite sign. The existence of a positive root means that the basic uniform gradient is unstable. This instability is easy to interpret. In the unstable modes, "strong" interfaces, characterized by larger $(\Delta T, \Delta S)$ monotonically grow at the expense of weaker interfaces. Numerical solutions of fully nonlinear equations governing the two-layer system indicate that unstable perturbations do not equilibrate until the weaker interface is completely eliminated. In essence, (8.16) represents the mergers of adjacent layers, such as realized in the DNS of staircases (Figs. 8.20–8.22).

While the foregoing merging model explains coarsening of staircases, it still fails to address one critical dynamical element – their eventual equilibration. The growth rate equation (8.16) suggests that as long as the density ratio is sufficiently low ($\bar{R}_\rho < R_{\min}$), the weaker interfaces will be sequentially eliminated. In this scenario, the number of steps continually decreases and the average step thickness increases correspondingly. What then prevents staircases from evolving to the ultimate state consisting of only one high-gradient interface separating two very deep mixed layers? One possibility is that continuous mergers in the equilibrium state could be balanced by splitting of steps – the idea originally advocated by Kelley (1988). However, recent observations (Timmermans *et al.*, 2008) and simulations (Prikasky, 2007; Noguchi and Niino, 2010a,b; Stellmach *et al.*, 2011) indicate that layer-splitting events in staircases are rare and unlikely to play a significant role in the step-size selection. Mergers simply stop when layers become sufficiently thick.

The hypothesis proposed by Radko (2005) invokes the slight inhomogeneity of the convecting layers (an effect ignored by the earlier layer-merging models) as a stabilizing agent controlling the equilibrium height of steps. Taking into account property variations across layers $(\Delta T_L, \Delta S_L)$ requires parameterization of the convective fluxes. Conventional wisdom (e.g., Turner, 1979) suggests that

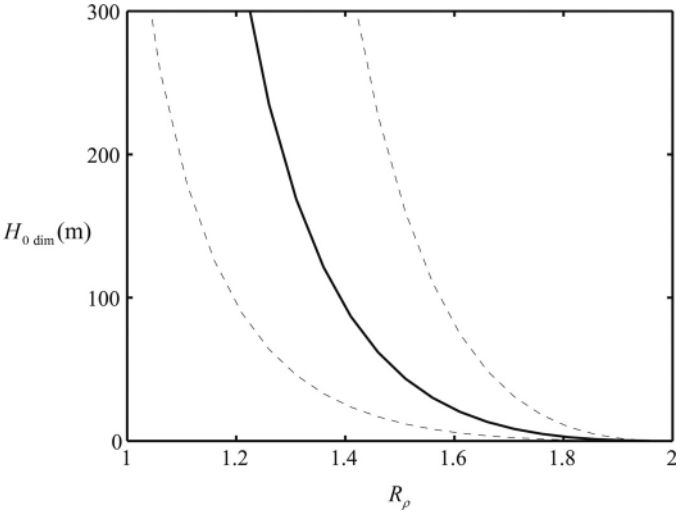

Figure 8.24 The dimensional equilibrium layer thickness as a function of the background density ratio as predicted by layer-merging theory for a fixed background temperature gradient of $\bar{T}_z = 0.03\ ^\circ\mathrm{C\,m^{-1}}$. Dashed lines indicate the plausible range of values due to the uncertainty in the model parameters. From Radko (2005).

the most important parameter controlling the strength of convective mixing is the density-based Rayleigh number:

$$Ra_\rho = \frac{g}{k_T \nu}\frac{\Delta\rho}{\rho}H_{\mathrm{dim}}^3. \tag{8.17}$$

Further assuming that the eddy diffusivities of heat and salt in convecting layers are equal and uniquely determined by (8.17) makes it possible to reproduce the stability calculation for finite $(\Delta T_L, \Delta S_L)$. The new stability model suggests that relatively thin layers successively merge as predicted by the earlier theory (Huppert, 1971; Radko, 2003). However these mergers cease when the thickness of layers exceeds a critical value (H_0), which, in turn, is controlled by background stratification. This critical thickness corresponds to the actual observed step size in fully equilibrated staircases.

Figure 8.24 presents a (dimensional) estimate of the critical thickness based on the layer-merging formulation of Radko (2005) as a function of the density ratio for typical oceanic conditions. Note the dramatic decrease in $H_{0\ \mathrm{dim}}$ with increasing R_ρ. This pattern, as well as the range of layer heights in Figure 8.24 (0–300 m) is generally consistent with observations. For $R_\rho = 1.6$, for example, the model predicts the scale of 20 m, which is close to the thickness of layers observed in the tropical North Atlantic, whereas very thick layers of 300 m and more have been

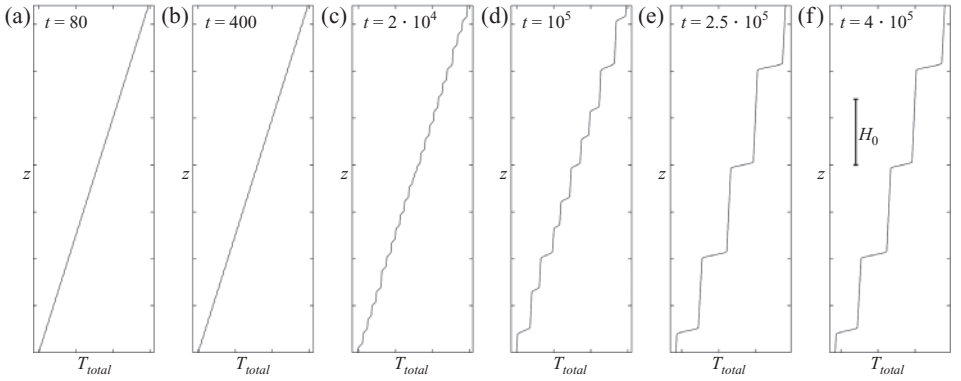

Figure 8.25 Formation and evolution of layers in an experiment with the parameterized vertical fluxes. Note the appearance of mixed layers separated by thin stratified interfaces, followed by a series of merging events, and their eventual equilibration. The dimensional critical thickness of layers evaluated for typical oceanographic parameters is $H_{0\,dim} \sim 20$ m. From Radko (2005).

observed in the Tyrrhenian Sea (Zodiatis and Gasparini, 1996) where the density ratio is anomalously low ($R_\rho \approx 1.2$). The uncertainty in theoretical estimates of the equilibrium thickness (indicated by dashed lines in Fig. 8.24) is large. It is primarily associated with the poorly constrained relation between the vertical T–S transport through the convective layers in oceanic staircases and $(\Delta T_L, \Delta S_L)$. However, the general pattern of the equilibrium thickness, characterized by the rapidly decreasing $H_{0\,\mathrm{dim}}(R_\rho)$, appears to be structurally robust.

Support of the merging theory is provided by the fully nonlinear numerical solution of the one-dimensional equations (8.8) in Figure 8.25. In this calculation, the diffusivities of heat and salt are assumed to be controlled by the density ratio in the salt-finger regions ($T_z > 0,\ S_z > 0,\ \rho_z < 0$) and by the Rayleigh number (8.17) in the convecting layers ($\rho_z > 0$). As expected, the layers that emerge first (Fig. 8.23b) are thin and unsteady. Figures 8.25c–e illustrate the subsequent evolution of a staircase: the steps merge continuously. Mergers occur when sufficiently strong interfaces, characterized by large temperature and salinity jumps, grow further, while weaker interfaces decay and eventually disappear, in accord with the layer-merging theory. The number of steps decreases and their characteristic vertical scale increases correspondingly. However, as time progresses, the coarsening of layers becomes less rapid and eventually stops completely. The variation in properties across convecting layers is critical in this regard; failure to take it into account leads to the final state with only one interface within the computational domain. No visible changes in the temperature field occurred between $t = 2.5 \cdot 10^5$ (standard non-dimensional units) in Figure 8.25e and $t = 4 \cdot 10^5$ in Figure 8.25f, suggesting

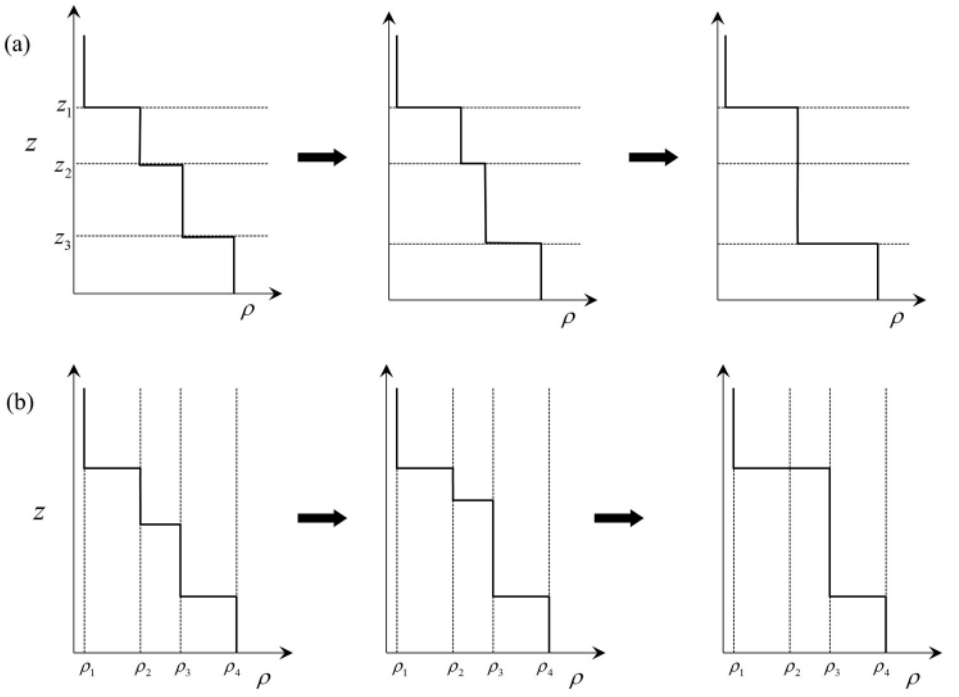

Figure 8.26 Schematic representation of the two possible merging scenarios: (a) the *B*-merger, which occurs when some interfaces gradually erode without moving vertically; and (b) the *H*-merger, which occurs when the interfaces drift vertically and collide. Numerical simulations and field data indicate that *B*-mergers are more common in thermohaline staircases.

that the staircase reached a stable state. The coarsening of the staircase was arrested only when the thicknesses of all layers exceeded the critical value H_0 predicted by the theoretical two-layer model.

The process of staircase equilibration is a lengthy one. In dimensional units, evaluated for typical oceanic scales, the equilibrium state in Figure 8.25e was reached by $t_{\text{dim}} \sim 2.5$ years, exceeding the fingering scale by approximately five orders of magnitude. Such slow predicted evolution of thermohaline staircases is supported by some oceanographic observations – see, for example, Figure 8.6 for the Tyrrhenian staircase.

Two other generalizations of the layer-merging theory should be mentioned. The first one concerns the evolutionary pattern of steps (Radko, 2007; Prikasky, 2007). The schematic in Figure 8.26 illustrates two principal merging mechanisms: (i) the *B*-merger, involving the decay and eventual disappearance of relatively weak interfaces (Fig. 8.26a) and (ii) the *H*-merger, characterized by the vertical

drift and collision of adjacent interfaces (Fig. 8.26b). These two merger types are manifestations of two distinct modes of instability, which are, in turn, controlled by the form of the interfacial flux laws. The instability producing *B*-mergers is caused by the variation in *T*–*S* fluxes as a function of property jumps across the steps $(\Delta T, \Delta S)$, whereas the *H*-instability occurs when fluxes respond to the changes in step height. If the staircase parameters are such that both instabilities are present, the evolutionary pattern is controlled by the instability with the larger growth rate. Whilst mergers through the elimination of weak interfaces (*B*-mergers) are clearly more common, numerical simulations (e.g., Noguchi and Niino, 2010b) indicate that *H*-mergers are possible for relatively thin steps in newly formed staircases. As layers grow in size, fluxes become largely insensitive to the step height – the spatially separated interfaces hardly affect each other – and therefore the *H*-instability is either absent or very weak. Thus, the late evolutionary stages of staircases and their ultimate equilibration are likely to be controlled by the *B*-merger dynamics.

Another point we wish to make regarding generalizations of the layer-merging theory concerns the parameterization of the interfacial fluxes. The most common versions of the model are based on Turner's 4/3 flux laws (Chapter 4). However, the risk of overreliance on these laws in certain configurations and parameter regimes cannot be ignored. Mergers in the staircase are driven by subtle imbalances of fluxes in the adjacent layers, which can potentially lead to the amplification of the errors associated with the assumed flux laws. This problem motivates a more general formulation of the layer-merging theory (Radko, 2007; Prikasky, 2007). Suppose for a moment that the *T*–*S* fluxes across each step are controlled by the property variations $(\Delta T, \Delta S)$ and the step height (H) in some unique but yet unspecified manner:

$$\begin{cases} F_T = F_T(\Delta T, \Delta S, H), \\ F_S = F_S(\Delta T, \Delta S, H). \end{cases} \tag{8.18}$$

In this case, it is possible to reproduce the layer-merging theory without making specific assumptions about the pattern of the one-step flux laws (8.18). The growth rate equation for *B*-mergers becomes

$$\lambda_B^2 + \frac{4}{H}\left(\frac{\partial F_T}{\partial \Delta T} + \frac{\partial F_S}{\partial \Delta S}\right)\lambda_B + \frac{16}{H^2}\left(\frac{\partial F_T}{\partial \Delta T}\frac{\partial F_S}{\partial \Delta S} - \frac{\partial F_S}{\partial \Delta T}\frac{\partial F_T}{\partial \Delta S}\right) = 0. \tag{8.19}$$

If the appropriate one-step flux laws are known or could be determined (numerically for instance), then the generalized merging theory (8.19) opens an attractive opportunity to theoretically predict the evolution of staircases and their ultimate equilibration.

We conclude the discussion of recent conceptual models of staircases with a cautiously optimistic summary. The instability of the flux-gradient laws mechanism (Section 8.3) and the associated layer-merging models explain several aspects of observations and find support in numerical simulations. The component of theory addressing the step-size selection is still somewhat hypothetical and qualitative. However, the model predicts the right range of scales and could possibly define the way forward by systematically refining its formulation. On the other hand, we should keep in mind that, for half a century, the theory of thermohaline staircases has served as a graveyard of interesting ideas and seemingly plausible explanations. It remains to be seen whether the most recent theory withstands more rigorous tests by field and laboratory experiments.